

Theory of the martensitic phase transformations in lithium and sodium

O. Blaschko

*Institut für Experimentalphysik, Universität Wien, Strudlhofgasse 4, A-1090 Wien, Austria
and Laboratoire Léon Brillouin, Centre d'Etudes Nucléaires de Saclay, F-91191 Gif sur Yvette, France*

V. Dmitriev

Faculty of Physics, Rostov State University, Rostov-on-Don, 344090 Russia

G. Krexner

*Institut für Experimentalphysik, Universität Wien, Strudlhofgasse 4, A-1090 Wien, Austria
and Laboratoire Léon Brillouin, Centre d'Etudes Nucléaires de Saclay, F-91191 Gif sur Yvette, France*

P. Tolédano*

Institut für Experimentalphysik, Universität Wien, Strudlhofgasse 4, A-1090 Wien, Austria

(Received 26 May 1998)

A phenomenological model is proposed which describes the static and dynamical properties observed in connection with the martensitic transformations in lithium and sodium. The martensite structure is shown to result from a coupling between the mechanisms associated with the bcc-9R, bcc-hcp, and bcc-fcc transformations. These mechanisms are expressed in terms of primary displacive order parameters, involving definite critical shifts, and of additional spontaneous symmetry breaking strains. The theoretical phase diagrams in which the bcc and martensite phases are inserted are worked out. They contain regions of stability for intermediate phases. The existence or absence of softening of the Σ_4 phonon branch with temperature, as a precursor effect to the transformation, is shown to depend on the distance of the experimental thermodynamic path to the corresponding intermediate phase. The nonlocalized character of the softening region on the Σ_4 branch reflects the coupling of the different structural mechanisms involved in the transformation. The irrational values found for the wave vectors at the phonon dips are interpreted by an implicitly incommensurate character of the transformation, which originates from the distinct coherency stresses between the potentially stable close-packed structures and the bcc matrix. It results in the creation of strain fields acting inhomogeneously on the effective transformation order parameter, and explains the observed incubation times and response of the crystals to elastic and plastic deformations. These properties are shown to be consistent with a nucleation process on elastic defects which is activated only close to the transformation.

[S0163-1829(99)04413-6]

I. INTRODUCTION

Martensitic transformations¹ constitute a very heterogeneous family of first-order structural transitions. This family includes several classes of transitions exhibiting distinct properties and mechanisms ranging from the slightly discontinuous transitions found in the A15 compounds² to the most strongly reconstructive (group-subgroup unrelated) transitions which take place in several elemental crystals.³

The essential features currently assumed for recognizing martensitic transformations are (1) the displacive (diffusionless) character of their atomistic mechanism, (2) the important role played by shear strains for obtaining the martensitic phase, (3) the specific transformation kinetics which involves precursor effects (e.g., typical nucleation processes, phonon anomalies, etc.) incubation times, and large regions of coexistence between the phases above and below the transition. However, some of these properties are often absent among transformations traditionally classified as martensitic. On the other hand many non-martensitic transitions possess some of the preceding features, e.g., first-order ferroelastic transitions in insulators.⁴

The fact that after more than a century of experimental investigations of martensitic transformations a unifying the-

oretical picture could not emerge reflects the variety and complexity of the situations found among these transformations. But it also reflects the fact that the nature and symmetry of the transformation order parameters have not been well understood and related organically to the proper critical variables and thermodynamic functions. This is the case, in particular, for the martensitic transformations in lithium and sodium to which the present article is devoted. We will show that a coherent theoretical description of most of the experimental features of the transformations in Li and Na can be deduced from the specific nature of the corresponding symmetry-breaking mechanisms.

A number of neutron scattering investigations of lithium and sodium by Smith and co-workers⁵⁻¹⁰ and Blaschko and co-workers¹¹⁻¹⁵ have recently added decisive finishing touches to the controversial picture of the transformations which occur at about 35 K in Na and 77 K in Li. One of the essential points which has been under discussion is the structure of the low-temperature (martensite) phases. Based on the evaluation of x-ray powder data these were initially described^{16,17} to consist of faulted hcp structures coexisting with a large amount of untransformed bcc matrix. A neutron diffraction experiment on Li by McCarthy *et al.*¹⁸ showed that powder data could not be well indexed by the double-

layered hcp stacking. Overhauser¹⁹ proposed that a nine-layered rhombohedral (9R) polytype structure would provide a better account of the preceding data. Subsequent elastic neutron scattering studies of Li single crystals^{8,13} confirmed a faulted 9R structure but further diffuse neutron scattering experiments^{14,15} revealed that the structure could be described as a complex arrangement of close-packed atomic planes exhibiting simultaneously various ordered stacking sequences. This disordered polytype structure coexists on cooling with the 9R and bcc structure whereas on heating above 80 K a fcc structure appears remaining as the only close-packed structure beside the bcc phase between 120 and about 180 K. The existence of a perfect fcc structure on heating that had been also obtained by Barrett after cold working of Li¹⁷ was independently confirmed in high-resolution experiments⁹ within the same temperature range both at 6.5 kbar and atmospheric pressure.

Although Na was initially regarded as equivalent to Li¹⁷ successive studies showed that its low-temperature phase was different in some respects. Thus, on the one hand, Schwarz *et al.*¹² found no short-range ordered polytype sequences but the coexistence of long-range ordered close-packed hcp, 9R, and bcc sequences whose relative volume fractions depend on temperature and specimen characteristics. On the other hand, Berliner *et al.*⁶ interpreted the crystallography of the low-temperature phase of Na as a complex mixture of almost hexagonal, rhombohedral polytypes with short and long periods forming a ladder of structures connected to one another by stacking faults. In both studies^{6,12} no fcc structure was reported.

Another important point of controversy concerns the lattice instabilities revealed by inelastic neutron scattering measurements on the Σ_4 phonon branch above the transitions. Although Smith *et al.*^{6,8,10} claimed that no evidence of transformation precursors could be observed in Na and Li Schwarz *et al.*¹⁵ reported in Li a partial softening of the acoustic [110] phonon branch polarized along $[1\bar{1}0]$ extending from $\mathbf{k}=0.1[110]$ to the surface of the Brillouin zone (the N point): from 200 to 100 K the softening increases towards the zone boundary whereas between 100 and 80 K it is accentuated near $\frac{1}{3}[110]$. In Na, Blaschko and Krexner¹¹ found the same phonon branch to soften close to and above $\mathbf{k}=0.4[110]$.

In the following sections we give a unified phenomenological description of the static (Sec. II) and dynamical (Sec. III) properties which characterize the martensitic transformations in sodium and lithium. In these sections we first clarify on a general basis the specific properties of the critical displacements, spontaneous strains (Sec. II) and phonon spectra (Sec. III) associated with martensitic ‘reconstructive’ transformations. In Sec. IV we summarize our results, differentiating the properties which are specific to Na and Li from the properties which hold more generally for any reconstructive transformation.

II. SYMMETRY AND THERMODYNAMIC ASPECTS OF THE PHASE TRANSFORMATIONS IN LITHIUM AND SODIUM

In this section we first show that the displacive mechanisms involved in the bcc-hcp, bcc-fcc, and bcc-9R transfor-

mations correspond to fixed critical atomic shifts (Sec. II A) which give to the hcp, fcc, and 9R phases a character of ‘limit’ states. We then infer the properties of the spontaneous strains which are necessary to obtain the hcp, fcc, and 9R structures to be symmetry-breaking quantities despite the fact that they are ‘secondary’ order parameters (Sec. II B). In Sec. II C we stress that the three preceding structures can also be obtained as the result of an ordering-type mechanism from a disordered hexagonal polytype parent structure. These properties are used to describe the structural and thermodynamic features reported for Na and Li on cooling and heating across their martensitic transformations (Sec. II D). We finally underline the specific nature of reconstructive martensitic transformations which appear to realize an intermediate situation between displacive-type and reordering-type mechanisms (Sec. II E). In all sections we use the labeling of Kovalev’s tables²⁰ for the bcc Brillouin zone (BZ) wave vectors and for the irreducible representations (IR’s) of the O_h^9 space group.

A. Limit martensitic phases

1. The bcc-hcp transformation

The bcc-hcp Burgers mechanism²¹ can be formulated^{3,22} in terms of a primary order parameter which consists in an antiparallel shifting of the atoms lying in the $(110)_{\text{bcc}}$ planes along the $\pm[1\bar{1}0]$ directions. As shown in Fig. 1(a) it leads to a doubling of the bcc unit cell with the following relationships between the hexagonal and cubic unit cell translations:

$$\mathbf{a}_h = \mathbf{a}_c + \mathbf{b}_c + \mathbf{c}_c, \quad \mathbf{b}_h = -\mathbf{c}_c, \quad \mathbf{c}_h = \mathbf{a}_c - \mathbf{b}_c. \quad (1)$$

The translational symmetry breaking expressed by Eq. (1) corresponds to one of the six branches $k_9^{(2)} = (\pi/a, -\pi/a, 0)$ of the star of the wave vector \mathbf{k}_9 which ends at the N -point of the bcc BZ boundary. On the other hand the antiparallel displacement field represented in Fig. 1(a) transforms as the basic function

$$\varphi(x, y) = (x + y)(\Delta_1 - \Delta_2 - \Delta_3 + \Delta_4 + \Delta_5 - \Delta_6 + \Delta_7 - \Delta_8), \quad (2)$$

where the Δ_i ’s are the shifts associated with the atoms numbered 1 to 8 in Fig. 1(a). $\varphi(x, y)$ has the symmetry of a one-dimensional IR ($\hat{\tau}_4$) of the little group D_{2h}^{xy} of \mathbf{k}_9 from which one can derive the six-dimensional IR, denoted $\hat{\tau}_4(\mathbf{k}_9)$ which accounts for the full sets of displacements from the O_h^9 space group at the N point. The equilibrium values of the corresponding six-component order parameter (η_i) ($i=1,6$) describing the displacement field of Fig. 1(a) are

$$\eta_2 = \eta \neq 0, \quad \eta_1 = \eta_3 = \eta_4 = \eta_5 = \eta_6 = 0. \quad (3)$$

They correspond³ to a phase of orthorhombic symmetry D_{2h}^{17} ($z=2$). The additional requirements for transforming the orthorhombic structure into the hcp structure (D_{6h}^4 , $z=2$) are the following.

(1) A specific critical magnitude for the antiparallel shifts ξ along $[110]$ given by

$$\xi_c = \frac{a\sqrt{2}}{12}. \quad (4)$$

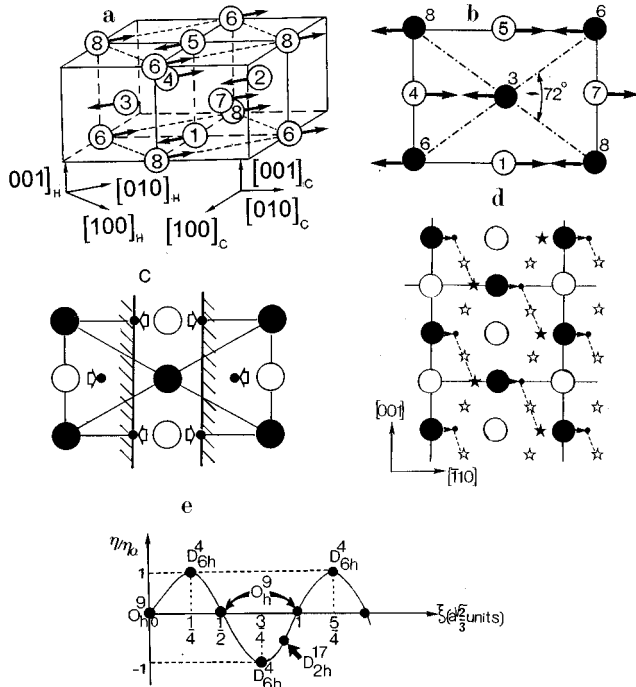


FIG. 1. (a) Average shifting of the atoms from the bcc to the hcp structures. The small cube (thick lines) is the bcc unit cell. The dotted parallelepiped is the unit cell of the orthorhombic D_{2h}^{17} structure. (b) bcc-hcp displacive mechanism in projection on the $(1\bar{1}0)$ cubic plane. After the shifts the angle between the diagonals of the rectangle becomes 60° . Solid and open circles are atoms located in two adjacent layers. (c) Creation of a geometrical barrier due to the contacts between atoms, which results in a reduction of the periodicity for the critical atomic displacements. (d) Projection of the bcc-hcp displacive mechanism on the (110) bcc plane. The shifting of atoms from their bcc positions (large circles) to their hcp positions (small dots) is $av\sqrt{2}/12$. The open and solid stars correspond to virtual positions at which the symmetry of the crystal would increase to O_h^9 and D_{6h}^4 , respectively. Solid and open large circles are atoms located in adjacent $(0$ and $\frac{1}{2})$ layers. (e) Periodicity of the order parameter $\eta(\xi)$ at the bcc-hcp transformation, following Eq. (7).

(2) A compression of the cubic unit cell along one of the fourfold axes (e.g., $[001]$) and a simultaneous decompression along the two other ($[100]$ and $[010]$) axes, which correspond to the combination of strain-tensor components

$$e_3 = \frac{1}{\sqrt{6}}(e_{xx} + e_{yy} - 2e_{zz}). \quad (5)$$

When the two preceding conditions are fulfilled the D_{2h}^{17} symmetry enlarges to D_{6h}^4 . This increase in the structural symmetry is illustrated in Fig. 1(b) which shows that the angle between the threefold axis in the $(1\bar{1}0)$ bcc planes which is $\arccos \frac{1}{3} = 70^\circ 32'$ in the cubic cell becomes 60° in the hexagonal cell.

Two additional ‘‘physical’’ constraints underlie the realization of the actual close-packed hexagonal structure.

(3) The interlayer distance d between the (110) cubic planes must be preserved in the hcp structure where they become the (001) hexagonal planes. This is a general prop-

erty of all elemental crystals undergoing a high-temperature bcc to low-temperature hcp transformation³ (i.e., in Ti, Zr, Hf, Be, Tl, ⁴He, Gd, Tb, Dy, Yb, Y) where the variation of d is found to be smaller than 1%. It implies the existence of a shear strain

$$e_6 = e_{xy} \quad (6)$$

which decreases the interlayer distance in the $[110]$ bcc directions (see Sec. II B).

(4) The size of the atoms has to be taken into account in the displacement field mechanism: one must exclude all shifts of the atoms after they have entered into contact. One can distinguish two types of contacts: (i) those which occur in the direction of the displacements such as between the pairs (3,4), (5,6), or (1,8) in Fig. 1(b) and (ii) those which take place in the perpendicular direction as between the pairs (4,8), (1,3) or (6,7) in Fig. 1(b). The role of the contacts between the atomic spheres is illustrated in Fig. 1(c). They create a geometrical barrier acting as a mirror plane perpendicular to the direction of the shifts.

Figure 1(d) represents, within the (110) bcc plane, the atomic shifting from the initial bcc positions to the final hcp positions. A striking property which can be foreseen from this figure is the periodic connection existing between the overall crystal symmetries undertaken by the structure and the virtual displacements ξ of the atoms along the $[110]$ direction. Thus, for general arbitrary displacements the structure exhibits the orthorhombic symmetry D_{2h}^{17} while for the critical displacements $\xi_c = av\sqrt{2}/12, 7av\sqrt{2}/12, 13av\sqrt{2}/12, \dots$, the structure acquires the D_{6h}^4 symmetry. For $\xi_c = 0, av\sqrt{2}/6, av\sqrt{2}/3, \dots$, one gets the bcc structure. This property has been justified within a more general framework in Ref. 23 and was shown to reflect the periodic dependence of the order parameter as a function of the critical displacements at reconstructive (group-subgroup unrelated) phase transitions. Assuming as usually that in the parent bcc structure $\eta = 0$ and that $\eta \neq 0$ for the orthorhombic and hcp structures one can express the functional dependence of η on ξ as

$$\eta(\xi) = \eta_0 \sin\left(\frac{6\pi}{av\sqrt{2}}\xi\right). \quad (7)$$

$\eta(\xi)$ is represented in Fig. 1(e). One can verify that, in agreement with our crystallographic description of the bcc-hcp mechanism, the intersection of the sinusoid with the ξ axis ($\eta = 0$) yields periodically the bcc symmetry for $\xi = 0, \frac{1}{2}, 1, \dots$ (in units of $av\sqrt{2}/3$) whereas the hcp symmetry coincides with the extrema of $\eta(\xi)$ for $\xi = \frac{1}{4}, \frac{3}{4}, \frac{5}{4}, \dots$. The other values of the order parameter η , associated with arbitrary shifts, correspond to the orthorhombic symmetry D_{2h}^{17} .

Using the transformation properties of the order parameter components (η_i) by the matrices of the IR $\tau_4(\mathbf{k}_g)$ and taking into account the equilibrium values of the η_i given by Eq. (3) one obtains^{3,4} the effective form of the order parameter expansion associated with the bcc-hcp transformation

$$F_1[\eta(\xi)] = F_{01}(P, T) + a_1 \eta(\xi)^2 + a_2 \eta(\xi)^4 + a_3 \eta(\xi)^6, \quad (8)$$

where $\eta(\xi)$ is expressed by Eq. (7). F_1 is expanded up to the sixth degree in $\eta(\xi)$ in order to account for a region of sta-

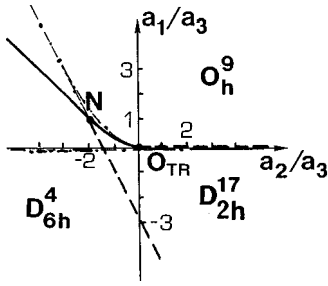


FIG. 2. Phase diagram associated with the order parameter expansion defined by Eq. (8). Full, dashed, and dash-dotted lines are, respectively, first-order, second-order, and limit of stability lines. N is a three-phase point. O_{TR} is a tricritical point.

bility including a direct first-order bcc-hcp transition line. The phenomenological coefficients in Eq. (8) are assumed to obey the usual conditions $a_1 = a_{10}(T - T_c)$ ($a_{10} > 0$) and $a_3 > 0$. The minimization of F_1 has to be performed with respect to the actual variational parameter ξ .²³ Therefore, the equation of state is

$$2\eta \frac{\partial \eta}{\partial \xi} (a_1 + 2a_2\eta^2 + 3a_3\eta^4) = 0 \quad (9)$$

yielding three possible stable phases for, respectively, $\eta = 0$ (the bcc phase), $\partial \eta / \partial \xi = 0$ (the hcp phase), and $\eta^2 = -[2a_2 + (4a_2^2 - 12a_1a_3)^{1/2}] / 6a_3$ for the ‘‘Landau’’ D_{2h}^{17} phase corresponding to a standard minimization of F_1 with respect to η . It thus confirms that the critical shifts associated with the bcc and hcp symmetries in the sinusoidal curve of Fig. 1(e) correspond to stable states.

Figure 2 represents the phase diagram resulting from the minimization of $F_1[\eta(\xi)]$ in the interval $0 \leq \xi \leq a\sqrt{2}/12$ in the plane of the phenomenological ratios $(a_1/a_3, a_2/a_3)$. The bcc-hcp transition is always first order, consistent with the absence of a group-subgroup relationship between the two phases. By contrast, the bcc- D_{2h}^{17} transition can be either first or second order in agreement with the fact that the phases are group-subgroup related. The three phases meet at the triple point N . Note that the critical displacements ξ are fixed in the hcp ($\xi_c^1 = a\sqrt{2}/12$) and bcc ($\xi_c^2 = 0$) phases whereas they vary between the extreme values ξ_c^2 and ξ_c^1 in the orthorhombic phase. In other words with respect to the critical displacements ξ the hcp and bcc phases appear as limit states.

2. The bcc-fcc transformation

Analogous properties as for the hcp phase can be found for the fcc phase at the bcc-fcc transformation mechanism. One can visualize the way a bcc lattice transforms into a fcc lattice via a deformation which stretches the bcc unit cell along one of the fourfold axes and compresses it to the same extent along the other fourfold axes. Such a macroscopic deformation which is shown in Fig. 3(a) is called the Bain deformation.²⁴ Figure 3(b) indicates the connection between the bcc and fcc (O_h^5 , $z=1$) unit cells. It corresponds to the following orientational relationships between the face-centered and body-centered unit cell basic vectors:

$$\mathbf{a}_1^F \parallel \mathbf{a}_c, \quad \mathbf{a}_2^F \parallel (\mathbf{a}_c + \mathbf{b}_c + \mathbf{c}_c), \quad \mathbf{a}_3^F \parallel (\mathbf{a}_c + \mathbf{c}_c). \quad (10)$$

This translational relationship is associated with a wave vector located at the center (Γ point) of the bcc BZ. The corresponding two-component order parameter³ coincides with the two combinations of the strain tensor components

$$\zeta_1 = e_3, \quad \zeta_2 = \frac{1}{\sqrt{2}}(e_{xx} - e_{yy}). \quad (11)$$

The Bain deformation is realized for the equilibrium values $\zeta_1 \neq 0$, $\zeta_2 = 0$. Hence, the same combination of strain tensor components e_3 , given by Eq. (5), which is an induced deformation in Burgers’ mechanism plays here the role of the symmetry-breaking quantity. For an arbitrary nonzero value of e_3 the bcc symmetry is lowered to D_{4h}^{17} which is also the symmetry of the ‘‘martensite’’ in carbon-steel alloys.¹ When the specific ratio $c/a = \sqrt{2}$ is realized, where a and c are the tetragonal lattice parameters, the preceding space group transforms into the face-centered cubic space group O_h^5 . The ratio $\sqrt{2}$ corresponds to a multiplication of the conventional bcc lattice parameters by $\sqrt{3}/2$ along the x and y axes and by $\sqrt{3}/2$ along z . Therefore, the numerical values of the spontaneous strain components which result in the Bain deformation are $e_{xx} = e_{yy} = \sqrt{3}/2 - 1$ and $e_{zz} = \sqrt{3}/2 - 1$ which yields $e_3 = 0.293$. Besides, in order to keep the atoms in contact at the transformation one needs to consider, as an additional secondary order parameter, the rigidity

$$e_1 = \frac{1}{\sqrt{3}}(e_{xx} + e_{yy} + e_{zz}) \quad (12)$$

which measures the decrease in volume at the transition. One finds $e_1 \approx -0.025$.

According to the preceding description the fcc phase appears to display, as the hcp phase, a character of limit phase: only for a fixed critical value of the order-parameter e_3 the fcc phase is obtained. We will now show that the bcc-fcc transformation has also, as the bcc-hcp mechanism, a periodic character. With that goal we will analyze the atomistic process which underlies the Bain deformation.

In the shearing deformation mechanism,²⁵ which is usually proposed as equivalent to the Bain deformation, the structural stability of the bcc structure is lowered with respect to an homogeneous shear strain of the (011) planes in the $\pm[0\bar{1}1]$ directions giving rise to the fcc structure. An experimental support for this alternative description of the bcc-fcc transformation is the decrease of the shear modulus $c_{11} - c_{12}$ observed in a number of bcc metals upon approaching the fcc phase.^{1,25} At the atomistic level the shearing mechanism can be decomposed into three successive steps which are shown in Figs. 3(c) and 3(d). (i) The layer containing the atoms numbered 7–12 in Fig. 3(c) is shifted by $a\sqrt{2}/6$ in the $[011]$ bcc direction, the atom in position 0 reaching the center of a triangle formed by the atoms denoted 8, 9, and 11. (ii) The next layer formed by the atoms 1–6 is subsequently shifted by $a\sqrt{2}/3$. This shifts the atom initially in 0 position to the center of the triangle of the following layer. (iii) At last, a shifting of the third layer by $a\sqrt{2}/2$ forces the atoms located in the layer to occupy equivalent positions, i.e., the corner atoms (0,0) lie on a straight line passing by the center of the triangles (8,9,11) and (2,4,5)

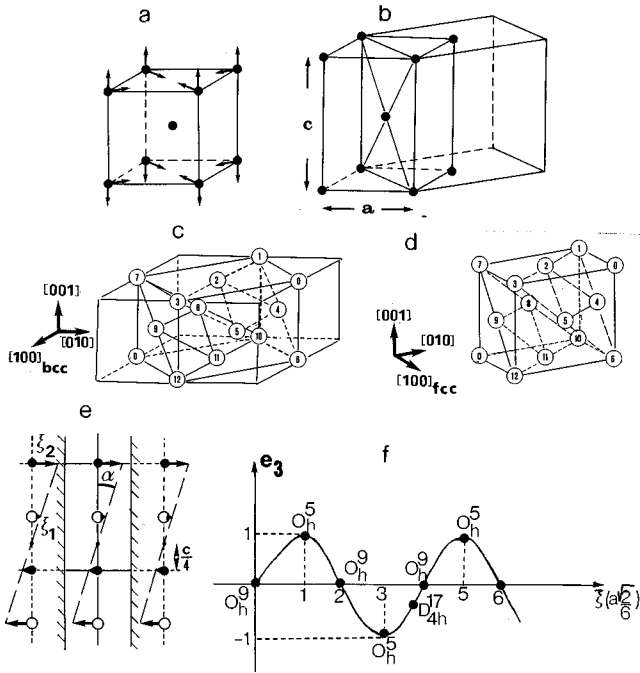


FIG. 3. (a) and (b): Macroscopic deformation representing the Bain deformation. (a) Corresponding atomic displacements. (b) Connection between the bcc and fcc unit cells. (c) and (d): Unit cells of the bcc (c) and fcc (d) structures. The numbering of the atoms is used in the description of the bcc-fcc transition mechanism given in the text. (e) Periodicity of the antiparallel shifting mechanism at the Bain deformation, with $\xi_n = (c/4)(2n+1)\tan\alpha$. (f) Periodic dependence of the order parameter following Eq. (13).

and orthogonal to the three successive layers. As a consequence, the layers containing the atoms labeled 0 in Fig. 3(c) become equivalent crystallographically. Thus, the resulting structure consists of a three-layered close-packed fcc structure represented in Fig. 3(d).

The preceding description of the Bain deformation at the atomistic level is very analogous to the description given for the Burgers mechanism since both mechanisms preserve the interlayer distance at the transformation. The essential difference is that in the Burgers mechanism two successive layers are shifted in opposite directions ($\mathbf{k} \neq 0$) whereas in the Bain deformation two successive layers are sheared in the same direction ($\mathbf{k} = 0$).

The periodicity of the atomic displacements corresponding to the bcc-fcc transformation is represented in Fig. 3(e). The mechanism can be depicted in terms of antiparallel displacements of the $(\bar{1}10)$ bcc atomic planes in the $\pm[110]$ directions. In this view a zero shift is chosen at the middle of the distance between two arbitrary planes, successive planes corresponding to increasing shifts $\xi_n = c/4(2n+1)\tan\alpha$ for the n th plane. α is the angle between the z axis and the direction formed by the shifted atoms [Fig. 3(e)]. The periodic relationship between the order parameter e_3 and the displacements ξ in the $\pm[110]$ directions can be expressed³ as

$$e_3 = e_3^0 \sin\left(\frac{3\pi}{a\sqrt{2}}\xi\right). \quad (13)$$

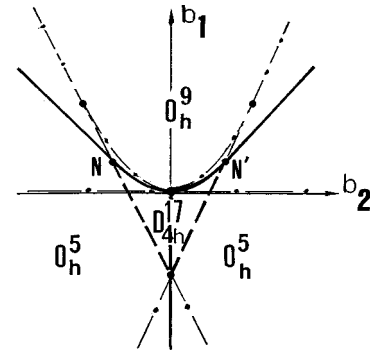


FIG. 4. Phase diagram associated with the order parameter expansion defined by Eq. (14). Full, dashed, and dash-dotted lines have the same meaning as in Fig. 2. N and N' are three-phase points. The two symmetric fcc regions correspond to antistructural phases.

The dependence of e_3 on ξ is shown in Fig. 3(f). One can verify that the bcc phase corresponds to the intersection of the sinusoidal curve with the ξ axis for the critical shifts $\xi_c = 0, 2, 4, \dots$ (in units of $a\sqrt{2}/6$) while the fcc structure coincides with the extrema of the curve for $\xi_c = 1, 3, 5, \dots$. All other values of ξ and e_3 give rise to the tetragonal D_{4h}^{17} phase.

Using the transformation properties of the two-component order parameter (ζ_1, ζ_2) given by Eq. (11), the equilibrium condition ($\zeta_1 \neq 0, \zeta_2 = 0$) and the form of $\zeta_1 = e_3$ given by Eq. (13) one obtains the effective order parameter expansion associated with the bcc-fcc transformation

$$F_2[\eta_3(\xi)] = F_{02}(T, P) + b_1 e_3(\xi)^2 + b_2 e_3(\xi)^3 + b_3 e_3(\xi)^4 \quad (14)$$

which can be restricted to the fourth degree in $e_3(\xi)$ since it contains a cubic invariant. The corresponding phase diagram is shown in Fig. 4 in the (b_1, b_2) plane. The phase diagram is symmetric with respect to the b_1 axis and, therefore, contains two possible regions of stability (for $b_2 > 0$ and $b_2 < 0$) for the fcc and intermediate tetragonal phases which are separated by a first-order isostructural transition line. Note that the full sequence of $\text{bcc} \rightarrow D_{4h}^{17} \rightarrow \text{fcc}$ transformations is realized in plutonium and protactinium²⁶⁻²⁸ and that a fcc-fcc isostructural transformation occurs in cerium.²⁹

3. The bcc-9R transformation

The preceding unifying scheme also applies to the bcc-9R transformation. The current mechanism for this transformation was proposed by Wilson and de Podesta.³⁰ It consists in a shifting of unequal amounts in the $[110]$ bcc direction of the atoms pertaining to nine successive bcc layers [Fig. 5(a)]. However, when taking into account the displacement associated with the tensile strain e_3 one can again describe the bcc-9R mechanism as a displacement field with antiparallel displacements of equal magnitude $a\sqrt{2}/6$, each third bcc layer remaining unshifted. For such critical shifts the monoclinic structure of symmetry C_{2h}^3 ($z=3$) which is obtained for general arbitrary displacements along $[1\bar{1}0]$ becomes the rhombohedral 9R structure. Note that the corresponding space group D_{3d}^5 ($z=3$) is not a subgroup of O_h^9 since its threefold axis is parallel to the $[110]$ direction and does not coincide with the threefold axis of the bcc structure. In the

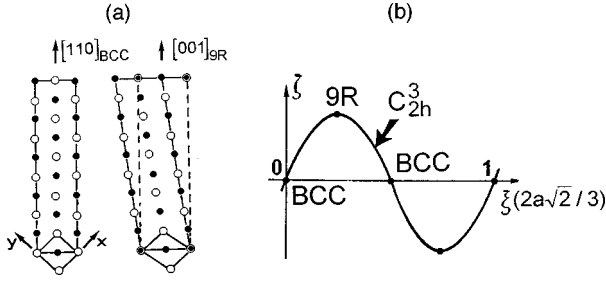


FIG. 5. (a) bcc-9R transformation mechanism following the description of Wilson and de Podesta (Ref. 30). (b) Dependence of the order parameter as a function of the critical displacements at the bcc-9R transformation, following Eq. (16).

preceding description the symmetry-breaking mechanism is associated with a twelve-dimensional IR of the O_h^9 space group denoted²⁰ $\tau_3(\mathbf{k}_4)$ with $\mathbf{k}_4 = (\pi/a, \pi/a, 0)$. The corresponding twelve-component order parameter (ζ_i) ($i = 1 \dots 12$) takes in the 9R phase the equilibrium values

$$\zeta_1 = \zeta_2 = \zeta \neq 0, \quad \zeta_i = 0 \quad \text{for } i = 3-12. \quad (15)$$

The dependence of ζ on the critical displacements ξ along $[1\bar{1}0]$ has the same periodicity as $e_3(\xi)$:

$$\zeta(\xi) = \zeta_0 \sin\left(\frac{3\pi}{a\sqrt{2}}\xi\right). \quad (16)$$

Figure 5(b) represents the $\zeta(\xi)$ periodicity with the successive onset of bcc, monoclinic and 9R sequences of phases. Using the transformation properties of the ζ_i ($i = 1-12$) by the IR $\tau_3(\mathbf{k}_4)$ and the equilibrium conditions (15) one can construct the order parameter expansion

$$F_3[\zeta(\xi)] = F_{03}(T, P) + c_1\zeta(\xi)^2 + c_2\zeta(\xi)^4 + c_3\zeta(\xi)^6. \quad (17)$$

$F_3(\zeta)$ is formally identical to $F_1(\eta)$. Accordingly the same topology as shown in Fig. 2 will hold for the phase diagram resulting from the minimization of $F_3[\zeta(\xi)]$ with respect to ξ , the 9R and monoclinic C_{2h}^3 phases replacing, respectively, the hcp and D_{2h}^{17} phases in Fig. 2.

B. Improper symmetry breaking strains

In our description of the bcc-hcp transformation mechanism we have shown that beyond the primary displacive mechanism additional spontaneous strains have to be taken into account in order to obtain the actual hcp structure. These strains couple to the order parameter and the corresponding coupling terms have to be added to the expansion $F_1[\eta(\xi)]$ given by Eq. (8). In the case of the bcc-hcp transformation, for example, identification of the relevant strains is obtained⁴ by decomposing the symmetrized second power of the IR $[\tau_4(k_9)]^2 \cong A_{1g} + E_g + F_{2g}$, where A_{1g} , E_g , and F_{2g} are, respectively, one-, two-, and three-dimensional IR's of O_h in the standard Landau notation.³¹ These IR's are spanned by the following combinations of the strain tensor components.

(i) A_{1g} corresponds to the rigidity e_1 [Eq. (12)] expressing a possible change in volume at the transition.

(ii) E_g transforms as the tensile strains (ζ_1, ζ_2) [Eq. (11)] associated with the Bain deformation of the bcc unit cell

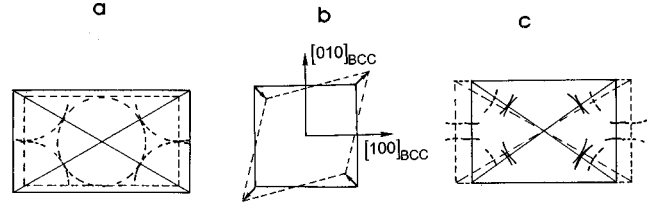


FIG. 6. Effect of the macroscopic strains e_3 (a) and e_6 [(b) and (c)] on the bcc unit cell. (a), (b), and (c) show projections on the $(\bar{1}10)$, (001) , and $(\bar{1}10)$ bcc planes, respectively. Dashed lines represent deformed states with respect to undeformed bcc structure in solid lines.

($\zeta_1 = e_3 \neq 0$, $\zeta_2 = 0$). Figure 6(a) illustrates the effect of e_3 which is to restore the close packing both inside the layers (e_{zz}) and between layers ($e_{xx} + e_{yy}$).

(iii) F_{2g} has the symmetry of the triplet (e_{yz}, e_{xz}, e_{xy}) describing a modification of the interlayer distance. In the hcp phase $e_{yz} = e_{xz} = 0$, $e_{xy} = e_6 \neq 0$. Figures 6(b) and 6(c) show that e_6 provides no contact between the atoms in the $[001]$ bcc direction but decreases the interlayer distance in the $[110]$ direction. Therefore, the full thermodynamic potential describing the bcc-hcp transformation takes the effective form

$$F_1[\eta(\xi), e_i] = F_1[\eta(\xi)] + \eta(\xi)^2 (\delta_1 e_3 + \delta_2 e_6 + \delta_3 e_1). \quad (18)$$

At this point it has to be emphasized that in the standard approach to structural transitions⁴ a coupling term of the form $\eta^2 e_i$ reflects the ‘‘improper’’ nonsymmetry-breaking character of the spontaneous strain e_i . In our description of the bcc-hcp mechanism it has been actually shown that e_3 results in an increase (to D_{6h}^4) of the orthorhombic symmetry D_{2h}^{17} . Thus, in contrast to the property of secondary order parameters to be non-symmetry-breaking quantities, the secondary strains at the bcc-hcp transformation take part in the breaking of the symmetry. More precisely, they induce an ‘‘increase’’ of the structural symmetry and play the role of a distinct order parameter though they are induced by the primary order parameters. This apparent contradiction is resolved when noting that the coupling terms in Eq. (18) establish a connection between the macroscopic strains and the critical atomic shifts ξ_c . The large values of ξ_c occurring at the transformation give rise to large spontaneous strains. For example, assuming a pure bcc-hcp mechanism in Na would give the following numbers: $e_3 = -0.29015$, $e_6 = -0.1518$, $e_1 = 0.08625$, which is more than one order of magnitude larger than the numbers usually found in ferroelastic transitions.⁴ The same order of magnitude is found for the ‘‘improper’’ strains involved in the bcc-hcp transformation in all the elemental crystals,³ e.g., the compression e_{zz} is larger than 10% in Ti, Zr, or Yb and reaches values above 20% in Ba or ³He.

The property of improper strains to become symmetry-breaking quantities holds for all martensitic transformations of the reconstructive type,³ i.e., in which a group-subgroup relationship between the initial and final structures is lost. At the bcc-fcc transformation where the tensile strain e_3 is the primary order parameter analogous considerations yield

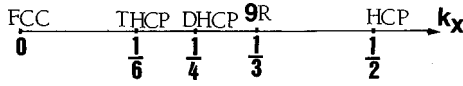


FIG. 7. Length of the k_x component of the wave vectors associated with the transformations from a bcc phase to a fcc(0), hcp($\frac{1}{2}$), 9R($\frac{1}{3}$), Dhcp($\frac{1}{4}$), or Thcp($\frac{1}{6}$) structure, on the Σ_4 line ($k_x, k_x, 0$) of the bcc Brillouin zone.

$$F_2(e_3, e_1, e_2) = F_2[e_3(\xi)] + \mu_1 e_3^2 e_1 + \mu_2 e_3 e_2^2 \quad (19)$$

in which the specific form of the μ_2 coupling reveals that shear strains (e_6) are not induced by spontaneous values of e_3 . For the bcc-9R transformation one finds

$$F_3[\zeta, e_i] = F_3[\zeta(\xi)] + \zeta^2(\nu_1 e_1 + \nu_3 e_6) + \nu_2 \zeta^3 e_3. \quad (20)$$

The same coupling invariants have been considered by Gooding *et al.*³² in their model of the bcc-to-9R transformation. However, these authors overlooked the symmetry-breaking character of the spontaneous strains and did not assume a dependence of the primary order parameter ζ on the critical displacements.

C. Disordered polytypes and transformations between closed-packed structures

The primary order parameter associated with the transformations from the bcc to the hcp, fcc, and 9R structures establish hexagonal ratios between the lattice parameters in (110) bcc layers and new translational symmetries in the [110] bcc directions. The corresponding wave vectors are located on the $\Gamma_5 - \Sigma_4 - N_4$ line of the bcc BZ. Figure 7 shows that along this line which coincides with the bisector ($k_x, k_x, 0$) of the (x, y) plane in reciprocal space, the fcc, 9R, and hcp structures are, respectively, obtained for $k_x = 0$, $k_x = \frac{1}{3}$, and $k_x = \frac{1}{2}$. Note that for the values $k_x = \frac{1}{4}$ and $k_x = \frac{1}{6}$ one may also get double and triple hcp structures which are found in several lanthanide elements.³ However, the fcc, 9R, and hcp hexagonal polytypes can also be obtained starting from a disordered hexagonal polytype structure.³³ We briefly describe this alternative possibility which will be used in our interpretation of the transformation mechanism in lithium.

Although a close packing of atoms represented by hard spheres may be realized in several ways,³⁴ in real crystals close packing always corresponds to a layered configuration which gives the possibility of isolating planes of atoms packed in the closest manner. In each layer any sphere is in contact with six nearest neighbors [position A in Fig. 8(a)]. In the centers of the triangles formed by neighbor atoms exist geometrically equivalent sites B and C. A spatially close packing is realized when each of the successive layers occupies the free spacings left by the preceding layers related to positions of the B or C type. The stacking order of the layers determines the close-packed structure. For stacked layers there exist geometrical conditions which reflect the close packing in three dimensions, namely, $c_h = a_h \sqrt{\frac{8}{3}}$ for a two-layer stacking (hcp structure), $c_h = a_h \sqrt{6}$ for a three-layer (fcc) stacking, etc.

The hcp and fcc structures which represent the simplest close packing configurations are represented in Figs. 8(b) and 8(c). Their unit cells are formed by two and three hex-

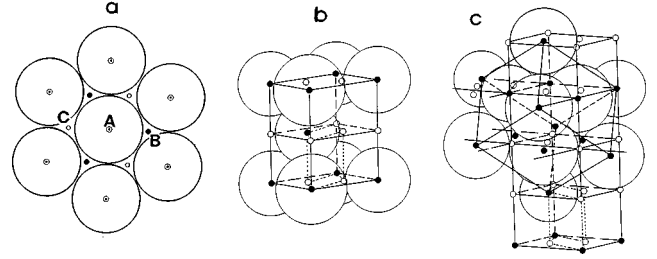


FIG. 8. (a) Projection of a close-packed layer of equiradii hard spheres on the (001) plane. A, B, and C represent atomic positions within the layer (A) and in the nearest adjacent layers (B and C). (b) and (c): unit cell of the disordered polytype structure, represented by dashed lines, within the hcp (b) and fcc (c) structures. Atoms are symbolized by large circles. The black and white small dots correspond, respectively, to atoms which are in equivalent positions in the polytype structure, and in inequivalent positions in the hcp and fcc structures.

agonal layers, each layer shifted with respect to the adjacent layers by $a_h \sqrt{3}$ in the [120] hcp direction where a_h is the basic vector of the rhombohedral fcc unit cell in hexagonal coordinates. From Figs. 8(b) and 8(c) one can foresee that the maximal substructure, common to the hcp and fcc structures, is composed by a monolayer hexagonal structure. This substructure denoted L hereafter corresponds to the hexagonal space group D_{6h}^1 with a unit cell volume $V_L = V_h/6 = V_c/3$, where V_h and V_c are the volumes of the hcp and fcc unit cells. The L unit cell which is shown within the hcp and fcc structures in Figs. 8(d) and 8(e) is filled by $\frac{1}{3}$ atom. It therefore corresponds to an occupancy $z = \frac{1}{3}$. This fractional number must be understood as follows: in a given L monolayer the atoms occupy the positions 1(a). Only one among the three A, B, and C positions in Fig. 8(a) is occupied in the monolayer. In the adjacent layers the atoms cannot be again in position A but only in position B or C, let us say B. In the following layers they occupy the position A or C and so forth. In other words the L -layer stacking realizes a statistically disordered polytype structure in which the A, B, and C sites are equivalent: the 1(a) positions are occupied with equal probabilities by atoms and vacancies.

Let us take the L -disordered polytype as the initial structure for describing the hcp and fcc structures. The relationship between the basic vectors of the hcp and fcc unit cells and the basic vectors ($\mathbf{a}_L, \mathbf{b}_L, \mathbf{c}_L$) of the L structure are

$$\mathbf{a}_h = 2\mathbf{a}_L - \mathbf{b}_L, \quad \mathbf{b}_h = \mathbf{a}_L + 2\mathbf{b}_L, \quad \mathbf{c}_h = 2\mathbf{c}_L \quad (21)$$

$$\mathbf{a}_c = \mathbf{a}_L + \mathbf{b}_L + \mathbf{c}_L, \quad \mathbf{b}_c = -\mathbf{a}_L + \mathbf{c}_L, \quad \mathbf{c}_c = -\mathbf{b}_L + \mathbf{c}_L. \quad (22)$$

From Eqs. (21) and (22) one can deduce the wave vectors expressing the breaking of the translational symmetry at virtual L -hcp and L -fcc transformations. One finds,²⁰ respectively, $\mathbf{k}_{15} = \frac{1}{3}(\mathbf{a}_L^* + \mathbf{b}_L^*) + \frac{1}{2}\mathbf{c}_L^*$ and $\mathbf{k}_{10} = \frac{1}{3}(\mathbf{a}_L^* + \mathbf{b}_L^* + \mathbf{c}_L^*)$, where \mathbf{a}_L^* , \mathbf{b}_L^* , and \mathbf{c}_L^* are the reciprocal lattice vectors of the L -hexagonal BZ.

\mathbf{k}_{15} coincides with the H point of the hexagonal BZ boundary. Since the hcp symmetry (D_{6h}^4 , $z=2$) is a subgroup of the L symmetry (D_{6h}^1 , $z=\frac{1}{3}$) one can find using a standard Landau approach^{3,35} that the L -hcp transition is as-

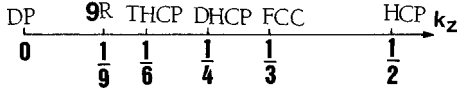


FIG. 9. Length of the k_z component of the wave vectors associated with the transformation from a disordered polytype (DP) phase to a $9R$ ($\frac{1}{9}$), hcp ($\frac{1}{2}$), fcc ($\frac{1}{3}$), $Dhcp$ ($\frac{1}{4}$), or $Thcp$ ($\frac{1}{6}$) structure, on the P line ($4\pi/3, 2\pi/3, k_z$) of the hexagonal Brillouin zone.

sociated with a two-component order parameter. The corresponding crystallographic mechanism involves a splitting of the initial [2(a)] onefold site into a threefold position 2(b), 2(c), and 2(d). After the transition, since the occupancy of the L structure is $\frac{1}{3}$, one of the preceding positions has to be occupied by two ($\frac{1}{3} \times 6$) atoms in the ordered hcp structure. As a result of close packing the hard sphere system of atoms can occupy either position 2(c) or 2(d) which are crystallographically equivalent. Therefore, the ordered crystal has a two-layered hexagonal close-packed structure with the standard ratio for the unit cell parameters $c_h/a_h = \sqrt{\frac{8}{3}}$.

The wave vector \mathbf{k}_{10} associated with the L -fcc translational relationship (22) is located on the edge of the hexagonal BZ of the L structure along the K - H line. Symmetry analysis^{3,35} shows that it gives rise to a threefold multiplication of the L unit cell corresponding to a rhombohedral structure of symmetry D_{3d}^5 ($z=1$). This structure coincides with the fcc symmetry when the ratio $c_L/a_L = \sqrt{2}$, expressing a close-packed structure is realized, which implies an angle of 60° between the \mathbf{a}_c , \mathbf{b}_c , and \mathbf{c}_c vectors.

According to the preceding description the hcp and fcc structures can be described as resulting from the transformations of a disordered polytype structure. Figure 9 shows that the \mathbf{k}_{15} and \mathbf{k}_{10} wave vectors used in these transformations lie on the same P line of the hexagonal BZ with coordinates ($4\pi/3, 2\pi/3, k_z$). For $k_z = \frac{1}{3}$ and $k_z = \frac{1}{2}$ the fcc and hcp structures are realized, respectively. It is immediate to show that the $9R$ structure coincides with $k_z = \frac{1}{9}$ whereas $k_z = \frac{1}{6}$ and $k_z = \frac{1}{4}$ correspond to the triple and double hcp structures.

D. The phase diagrams of sodium and lithium

The results obtained in Secs. II A–II C can be used as a basis for describing the phase diagrams of sodium^{6,12} and lithium.^{8,10,14} Let us first consider the experimental data reported by Schwarz *et al.*¹² for Na. The sequences of phases

observed by these authors on cooling and heating involve the bcc, $9R$, and hcp phases. Using the effective forms of the thermodynamic potentials associated with the bcc-hcp [Eq. (18)] and bcc- $9R$ [Eq. (20)] transformations one can write the total effective thermodynamic potential as

$$\Phi_1[\eta(\xi_1), \zeta(\xi_2), e_i] = F_1[\eta(\xi_1), e_i] + F_3[\zeta(\xi_2), e_i] + \gamma_1 \eta^2(\xi_1) \zeta^2(\xi_2), \quad (23)$$

where ξ_1 and ξ_2 denote the respective displacements occurring at the bcc-hcp and bcc- $9R$ transformation mechanisms. The γ_1 term is the lowest degree coupling invariant between the η and ζ order parameters.

The general features of the phase diagrams obtained by minimizing Φ_1 with respect to ξ_1 and ξ_2 are shown in Figs. 10(a) and 10(b) within the plane (c_1, a_1) of the phenomenological coefficients of the quadratic invariants in F_1 and F_3 . Since these coefficients depend linearly on temperature and pressure the topology of the transition lines and phases in Figs. 10 are preserved in the corresponding temperature-pressure phase diagrams. Note that a negative value has been assumed for the coefficients a_2 and c_2 . It implies that the intermediate Landau state in Fig. 2 is unstable. Figure 10(a) corresponds to a strong coupling between η and ζ ($\Delta = 4a_2c_2 - \gamma_1^2 < 0$) whereas Fig. 10(b) assumes a weak coupling ($\Delta > 0$) between the two order parameters. The two figures reveal that beside the $9R$ ($\eta=0, \zeta \neq 0$) and hcp ($\eta \neq 0, \zeta=0$) phases an additional phase corresponding to an 18-layer polytype structure ($18R$) can be stabilized for $\eta \neq 0, \zeta \neq 0$. This phase can be reached from the bcc phase either via the $9R$ or hcp phases [Fig. 10(a)] or directly across a first-order transition line [Fig. 10(b)] limited by two triple points T_1 and T_2 . The hatched areas in the figures represent regions of coexistence of two phases adjacent to first-order transition lines. Cross-hatched areas are regions of coexistence of three phases close to the triple points T_1 and T_2 .

Figure 11(a) focuses on the region of the phase diagram represented in Fig. 10(a) surrounding the triple point T_1 . The phase sequences indicated by the thick arrows 1 and 2 coincide with the thermodynamic paths followed by Schwarz *et al.*¹² in their diffuse neutron scattering investigation, which are schematically reproduced in Fig. 11(b). Thus, on cooling one goes from bcc to (bcc+ $9R$ +hcp) whereas on heating one gets successively the phase sequence (bcc+ $9R$ +hcp) \rightarrow (hcp+bcc) \rightarrow bcc. The difference in the phase se-

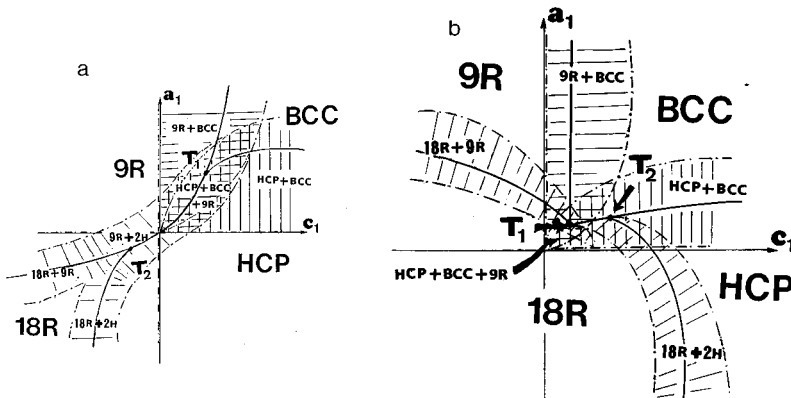


FIG. 10. Phase diagrams associated with the coupled order parameter expansion defined by Eq. (23). The description of the phase diagrams are in the text. Full and dash-dotted lines are, respectively, first-order and limit of stability lines. (a) corresponds to a strong coupling between the order parameters η and ζ , whereas (b) assumes a weak coupling.

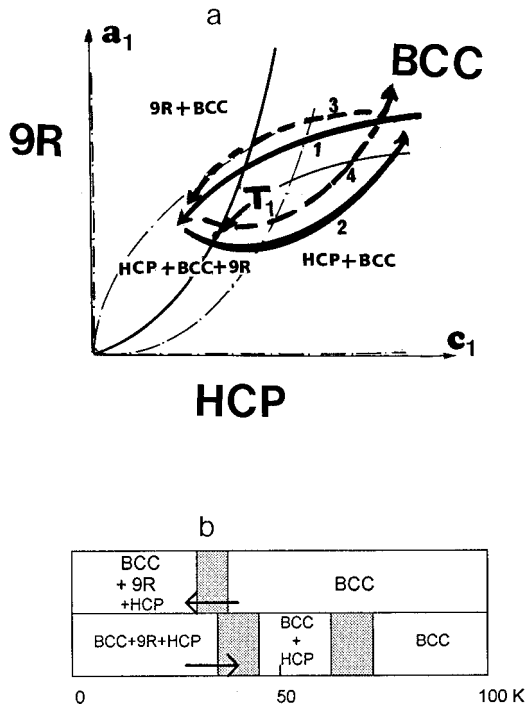


FIG. 11. (a) Region of the phase diagram of Fig. 10(a) surrounding the triple point T_1 . The arrows denoted 1 and 2 indicate the sequences of phases found in sodium (Ref. 12) which are represented in (b). The arrows denoted 3 and 4 show the evolution of the thermodynamic paths when cycling across the transformation.

quences on cooling and heating corresponds to a standard hysteretic behavior usually expected at first-order transformations. A less usual behavior which relates to the specific transformation kinetics in Na and Li (see Sec. III) is observed in a second cooling cycle during which Schwarz *et al.*¹² find a reduction in the amount of the hcp phase with an almost pure 9R phase coexisting with the bcc matrix. Therefore, cycling across the transition shifts the thermodynamic paths towards the pure 9R region as shown by the arrows 3 and 4 in Fig. 11(a). Such a tendency is consistent with the neutron powder diffraction study on Na by Berliner *et al.*¹⁰ who found a small fraction of hcp phase coexisting with large amounts of 9R and bcc phases.

In a further neutron diffraction study on single crystals Berliner *et al.*⁶ observed a more complex structure for the Na martensite that was interpreted either in terms of a two-component 9R+27R polytype mixture or in terms of a three-component 9R+15R+45R mixture. Let us show that the first of these interpretations can be simply justified in the framework of our approach by considering the ubiquitous role played by the tensile strain e_3 in the transformation mechanisms. The full effective thermodynamic potential associated with the coupled bcc-9R and bcc-fcc transformations can be written

$$\begin{aligned} \Phi_2[\zeta(\xi_2), e_3(\xi_3), e_i] = & F_3[\zeta(\xi_2), e_i] + F_2[e_3(\xi_3), e_i] \\ & + \gamma_2 \zeta^3(\xi_2) e_3(\xi_3) + \gamma_3 \zeta^2 e_3^2, \end{aligned} \quad (24)$$

where ξ_2 and ξ_3 are the displacements, respectively, associated with the bcc-9R and bcc-fcc transformation mecha-

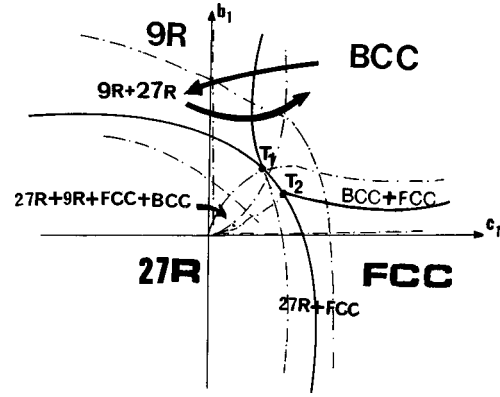


FIG. 12. Phase diagram associated with the coupled order parameter expansion defined by Eq. (24). The description of the phase diagram is given in the text. The same convention as in Fig. 10 is used for the transition and limit of stability lines. The arrows indicate the experimental path possibly followed by Berliner *et al.* (Ref. 6).

nisms. The γ_2 and γ_3 terms are the lowest degree couplings which have to be taken into account to insert the bcc, 9R, and fcc phases within the same phase diagram. The forms of F_3 and F_2 are given by Eqs. (14), (17), (19), and (20). Minimizing Φ_2 with respect to ξ_2 and ξ_3 yield the following equations of state:

$$\begin{aligned} \frac{\partial \Phi_2}{\partial \xi_2} = 2\zeta \frac{\partial \zeta}{\partial \xi_2} \left(c_1 + 2c_2 \zeta^2 + 3c_3 \zeta^4 + \frac{3}{2} \gamma_2 \zeta e_3 + \gamma_3 e_3^2 \right) = 0, \\ \frac{\partial \Phi_2}{\partial \xi_3} = e_3 \frac{\partial e_3}{\partial \xi_3} (2b_1 + 3b_2 e_3 + 4b_3 e_3^2 + 2\gamma_3 \zeta^2) + \gamma_2 \zeta^3 = 0. \end{aligned} \quad (25)$$

Assuming unstable intermediate Landau phases (of symmetries D_{4h}^{17} and C_{2h}^3), i.e., $|b_2| > b_2^0$ in Fig. 4 and $c_2 < 0$ one obtains the phase diagram represented in Fig. 12 in the (b_1, c_1) plane. In addition to the parent bcc phase ($\eta = \zeta = 0$) three phases possess a domain of stability. (1) The fcc phase which corresponds to $\zeta = 0$ and $\partial e_3 / \partial \xi_3 = 0$. It is realized for the fixed strain $e_1^S(\xi_3^c)$ where $\xi_3^c = a\sqrt{2}/6$ (see Sec. II A 2). (2) The 9R phase corresponding to $\zeta(\xi_2^c) \neq 0$ and $\partial \zeta / \partial \xi_2 = 0$. It is also realized for a fixed strain $e_2^S(\xi_2^c) \neq 0$ (see Sec. II A 3). (3) A 27R polytype structure obtained for $\zeta(\xi_2) \neq 0$, $e_3(\xi_3) \neq 0$ which is the minimal common superstructure for the fcc and 9R structures. It involves tensile strains e_3 varying between e_1^S and e_2^S .

In other words the stabilization of the 9R structure requires the existence of an improper (symmetry breaking) secondary strain e_3 due to the specific form of the nonlinear coupling term γ_2 . Since e_3 is also the primary order parameter giving rise to a fcc phase an intermediate 27R polytype structure may likewise possess a region of stability adjacent to the 9R phase. Figure 12 shows that the 9R and 27R polytypes coexist around the 9R-to-27R first-order transition line. The arrows on the figure symbolize the thermodynamic paths corresponding to the experimental observations of Berliner *et al.*⁶ The alternative interpretation of these authors of the structure of sodium martensite in terms of a three-component 9R+15R+45R mixture can also be in principle

obtained by analogous considerations. Since an improper coupling of the form $\gamma_4 \eta^2 e_3$ exists between the η and e_3 order parameters it may lead to the stabilization of a six-layer ($6H$) intermediate phase between the hcp and fcc regions. Therefore, the $15R$ and $45R$ polytypes should correspond to the regions of coexistence surrounding the $9R$ - $6H$ and $27R$ - $18R$ transition lines. However, such an interpretation would require the coupling between the three bcc-hcp, bcc- $9R$, and bcc-fcc order parameters and is physically less probable.

In summary, the structure of the Na martensite disclosed by Schwarz *et al.*¹² and Berliner *et al.*⁶ has been described by thermodynamic considerations involving the coupling between the mechanisms (order parameters) assumed in our approach for the bcc-hcp, bcc- $9R$, and bcc-fcc transformations. The description stresses the important role played by the tensile strain e_3 in these transformations which acts as a primary order parameter or as a secondary symmetry breaking quantity. It remains to understand why the thermodynamic paths partly differ in the two experimental studies. The most consistent explanation relates to the intrinsically faulted nature of the considered close-packed structures which has been stressed by Schwarz *et al.*¹² and serves as a basis for the structural analysis of the Na martensite by Berliner *et al.*⁶ The amount of stacking faults increases on cycling across the martensitic transformation, i.e., from virgin to deteriorated samples. At given temperature and pressure it shifts the phase fractions towards a larger amount of longer polytype sequences, e.g., from hcp to $9R$ as observed by Schwarz *et al.*¹² Besides, the concentration of stacking faults preexisting in virgin samples differs from one sample to another depending on sample preparation.

Let us briefly describe the type of intrinsic (symmetry induced) stacking faults expected at the bcc-hcp and bcc- $9R$ transformations. Such type of stacking faults results from the existence of antiphase domains which transform into one another by the translations lost at the transformation from the bcc structure. At the bcc-hcp transition (Sec. II A 1) the critical wave vector is $\mathbf{k}_9 = \frac{1}{2} \mathbf{c}_c^*$ where \mathbf{c}_c^* is the bcc reciprocal lattice vector. Hence two types of antiphase domains occur in the hcp structure transforming into one another by the bcc translation \mathbf{c}_c . The $ABABABAB \cdots$ stacking will therefore be changed into $ACACACAC \cdots$. The domain texture resulting from the existence of these two antiphase domains being compatible with a close-packed structure contains the sequences $ABABACAC \cdots$ and $ABABACAC \cdots$. They correspond, in Jagodzinski notation,³⁶ to the deformation stacking faults $hhhhchhh \cdots$ and $hhhcchhh \cdots$. Note that the first type of stacking fault is energetically more probable since only one irregular cubic layer is inserted.

The bcc- $9R$ transformation is associated with the wave vector $\mathbf{k}_4 = \frac{1}{3} \mathbf{c}_c^*$ (see Sec. II A 3) which gives rise to three types of antiphase domains transforming by the lost translations \mathbf{c}_c and $2\mathbf{c}_c$: $ABCBCACAB \cdots CABABCBCA \cdots$ and $BCACABABC \cdots$ corresponding to $hchhchhch \cdots$. The easier conjugation is $ABCBCACAB.CABABCBCA \cdots$ which can be written $hchhchhccchhchhch \cdots$. It coincides with the $H \wedge H$ stacking fault considered by Berliner and Werner.³⁷ A contact between $ABCBCACAB \cdots$ and

$BCACABABC \cdots$ is energetically unlikely since it would contain a BB sequence and at least one layer stacking should be missed.

The preceding analysis considers exclusively the stacking faults which can be predicted from the conjugation between symmetry induced antiphase domains composed by hcp or $9R$ unit cells. It does not take into account the stacking faults (growth faults) which may result from conjugation of partial stacking sequences that would give rise to more arbitrary polytype structures as discussed by Berliner *et al.*⁶ The main conclusion is that the hcp and $9R$ phases are intrinsically faulted as it has been emphasized in all the experimental observations of the Na martensite.^{6,12,37} Note in this respect that no symmetry induced stacking faults should be produced at the bcc-fcc transformation since the corresponding mechanism occurs at $\mathbf{k} = 0$, i.e., no bcc translation is lost.

In addition to antiphase domains the bcc-hcp and bcc- $9R$ transformation mechanisms give rise to specific distributions of orientational domains. The number and orientation of these domains does not follow the standard scheme³ since it is determined by the lowering of the bcc point group symmetry occurring in the intermediate Landau structures (orthorhombic or monoclinic) assumed in the transformation mechanisms. Thus the bcc-hcp transformation should give rise to *six* orientational domains since the point group (D_{2h} of the intermediate state (Sec. II A 1) allows six orthorhombic variants which transform into one another by the fourfold rotations lost at the transformation. Each variant transforms into an hcp domain under the effect of the tensile strain e_3 . At the bcc- $9R$ transformation the lowering of the bcc symmetry to C_{2h}^3 produces *twelve* orientational monoclinic domains along the $[110]$ and equivalent cubic directions. Due to the asymmetry of the coupling ($\zeta^3 e_3$) with the order parameter ζ the tensile strain e_3 , which restores the $9R$ close packed structure, splits each of the preceding domains in a pair of unequivalent domains symmetrically located with respect to the (110) and equivalent cubic planes. Accordingly, the $9R$ phase should display 24 orientational domains. This coincides with the 24 rhombohedral variants found about each of the bcc (110) planes by Berliner *et al.*⁶ The numbers found by these authors i.e., $(1.018, 0.92, \pm 0.06)$ provide a rough estimate of the magnitude of the e_3 strain involved in the bcc- $9R$ transformation.

The phase diagram of lithium differs in a number of aspects from the sodium phase diagram. The neutron diffraction studies of Smith *et al.*^{7,8,10} and Blaschko *et al.*^{13,14} analyze the Li martensite in terms of $9R$ structure coexisting with the bcc matrix. The two groups also find a long-range fcc structure which appears only on heating both at atmospheric pressure and at 6.5 kbar.^{8,14} The diffuse scattering analysis of a wider region of reciprocal space by Schwarz and Blaschko¹⁴ reveals that the long-range $9R$ phase coexists at low temperature with a disordered polytype structure where short-range ordering tendencies of hcp, fcc, and $9R$ phases are simultaneously present.

Let us emphasize that the observation of a fcc phase exclusively on heating above the region of stability of a disordered polytype phase strongly suggests that the mechanism described in Sec. II C applies, i.e., the existence of a disordered polytype structure is here a preliminary requisite for the formation of the fcc phase and plays the role of its parent

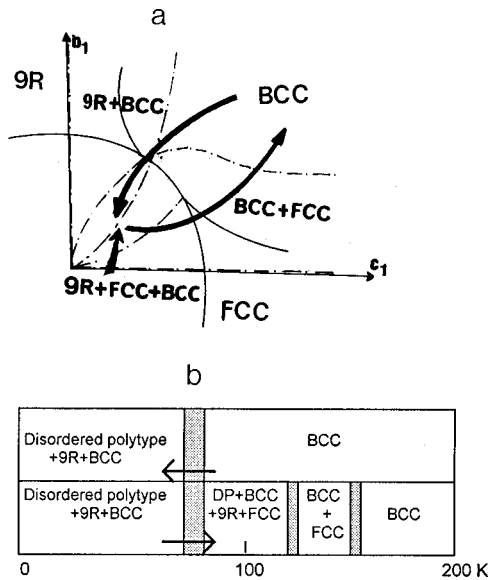


FIG. 13. (a) Region of the phase diagram of Fig. 12 surrounding the first-order transition line joining the triple points T_1 and T_2 . The arrows 1 and 2 show the phase sequences reported by Schwarz and Blaschko (Ref. 14) on cooling and heating, as represented in (b).

phase. Reference to the considerations developed for constructing the phase diagram of Fig. 12 shows that a long-range fcc structure adjacent to a long-range $9R$ structure and induced from the bcc phase cannot occur since the two structures require for their stabilization different fixed values of the tensile strain e_3 . A long-range $9R$ structure induces a disintegration of the fcc structure which may only survive under the form of short-range sequences leading ultimately to a fully disintegrated long-range disordered polytype structure. In contrast, the fcc structure formed on heating from the disordered polytype does not require specific values of e_3 for its stabilization and, therefore, may coexist with the $9R$ structure.

Figure 13(a) represents the region surrounding the T_1, T_2 line in Fig. 12. The arrows 1 and 2 reflect the phase sequences reported by Schwarz and Blaschko [Fig. 13(b)] on cooling and heating, respectively. On cooling one gets the $bcc \rightarrow (bcc + 9R + \text{disordered polytype})$ sequence whereas on heating the $(\text{disordered polytype} + bcc + 9R + fcc) \rightarrow (bcc + fcc) \rightarrow bcc$ sequences are obtained.

E. Intermediate nature of the mechanism in martensitic reconstructive transformations

The transition mechanisms described in Sec. II A have been expressed in terms of atomic displacements in agreement with the displacive character usually assumed for martensitic transformations.¹ However, reconstructive martensitic transformations realize in some respects an *intermediate situation between displacive and ordering processes*. In order to make this point more clear we will first recall the current schemes assumed for ordering and displacive mechanisms.

A system undergoing a purely ordering-type transition can be considered as a set of positions, fixed in space, and filled by heterogeneous objects: atoms and vacancies, or at-

oms and ions of different elements, etc. The ordering process causes a change in the distribution of objects among the positions but does not displace the positions. Strictly speaking the symmetry of the probability distribution function of the objects is the result of averaging of the real atomic distribution as it is obtained from experiment. The coincidence between the distribution functions of the different types of particles and the actual distribution is realized in the fully ordered state. In systems undergoing a purely displacive transformation the crystallographic positions are fully occupied by identical particles which are shifted in the transformation process. This process induces a crystallographic inequivalence among atomic sites that were initially equivalent and no diffusion leading to an exchange of atoms takes place. There is also an important difference in the dynamics of ordering and displacive mechanisms: the diffusional motion of atoms in ordering processes is uncorrelated while the atomic shifts represent a collective process for displacive mechanisms.

Reconstructive martensitic transformations as described in Sec. II A correspond to an intermediate mechanism. On the one hand a displacive reconstructive transformation from the initial phase to a limit phase (e.g., bcc -hcp, bcc - $9R$, bcc -fcc, etc.) transfers atoms from one fixed site to another site without any intermediate position but the corresponding atomic shifts occur collectively. The intermediate nature of the mechanism clearly appears in transformations between close-packed structures. In a reordering mechanism between such types of structures (e.g., $hcp \leftrightarrow fcc$) the change in the position of an individual atom from the layer position A to the position B requires the creation of high-energy defects connected with the absence of vacant interstices. It is thus energetically more advantageous to shift simultaneously (collectively) all the atoms pertaining to the layer A . Furthermore, a relative displacement of layers appears as uncorrelated but has indeed correlations: if the original stacking of layers is random, e.g., $ABCBA \cdots$, and the second layer has to be shifted from position B to position C it causes a displacement of the successive layer which cannot occupy the C position in the new structure due to geometrical constraints. For example, in the fcc -hcp mechanism the reordering of the layers between the two structures has a clear correlation: the three-layered fcc periodic stacking $ABCABC \cdots$ has to be replaced by the two-layered $ABABAB \cdots$ stacking. This can be realized by periodically repeated shifts of each unshifted AB pair: CA moves in the direction $C \rightarrow A$ [Fig. 8(a)] and becomes AB while BC is displaced from B to A and also becomes AB . The next AB pair is unshifted, etc. Hence the reordering fcc -hcp process is periodically correlated.

In summary, reconstructive martensitic transformations allow a continuous crossover from ordering to displacive mechanisms. This is made possible by the invariability of the order parameter values in the two mechanisms: it is constant and maximal when going from a fully ordered state to a limit displacive state as defined in Sec. II A.

III. PRECURSOR EFFECTS

Before analyzing the experimental results reported for the lattice instabilities in Na and Li, as revealed by inelastic neutron scattering experiments^{6,7,9,11,13,15,45,38,39} (Sec. III B),

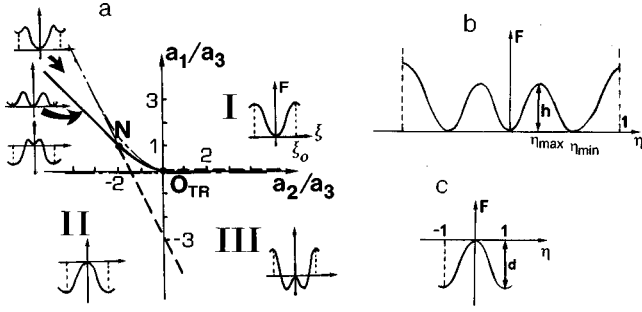


FIG. 14. (a) Form of the energy barrier in each relevant region of the phase diagram of Fig. 2. (b) Energy barrier along the bcc-hcp reconstructive transition line. h is the height of the barrier. (c) Depth d of the potential well in the hcp phase.

we describe the general dynamical properties which characterize reconstructive martensitic transformations in the framework of our approach (Sec. III A). The possible connections between the precursor instabilities and the transformation mechanism are discussed in Sec. III C. In Sec. III D a nucleation mechanism on elastic defects, adapted to the case of Li and Na, is formalized.

A. Phonons and martensitic reconstructive transformations

Let us first analyze the influence of the secondary strains on the height of the energy barrier at a reconstructive transformation using as an illustrative example the bcc-hcp transformation. The form of the energy barriers in each relevant region of the phase diagram of Fig. 2 is shown in Fig. 14(a). Figure 14(b) represents the energy barrier along the bcc-hcp transition line. This line is given by the equation $\partial\eta/\partial\xi = 0$, which yields $\eta = \eta_0$ from Eq. (7), and by the equality of the effective potentials $F_1(\eta=0) = F_1(\eta=\eta_0)$ where $F_1(\eta)$ is defined by Eq. (8). Therefore, the equation of the bcc-hcp transition line is

$$\frac{a_1}{a_3} = -\frac{a_2}{a_3} \eta_0^2 - \eta_0^4 \quad (26)$$

which corresponds to a straight line in the $(a_1/a_3, a_2/a_3)$ plane. The coordinates of the minima of the energy barrier in Fig. 14(b), associated with nonzero values of the order parameter, are

$$\eta_{\min} = \pm \eta_0, \quad (27)$$

whereas the coordinates of the closest maxima are

$$\eta_{\max} = \pm \frac{1}{\sqrt{3}} \eta_0. \quad (28)$$

From Eqs. (27) and (28) we can deduce the height h of the barrier

$$h = F_1(\eta_{\max}) - F_1(\eta_{\min}) = -\frac{2}{9} \eta_0^4 \left(a_2 + \frac{4}{3} a_3 \eta_0^2 \right). \quad (29)$$

which is a positive quantity since $a_2 < -2a_3 \eta_0^2$ in the region of stability of the hcp phase. In order to evaluate the influence of the secondary strains e_3 , e_6 , and e_1 on h one has to

use the full effective form of $F_1[\eta(\xi), e_i]$ given by Eq. (18) to which must be added the elastic energy associated with the strains e_3 , e_6 , and e_1 :

$$F_1^{\text{el}}(e_i) = \frac{1}{2} (c_{11} - c_{12}) e_3^2 + \frac{1}{2} c_{44} e_6^2 + \frac{1}{2} (c_{11} + 2c_{12}) e_1^2, \quad (30)$$

where the c_{ij} ($i=1-6, j=1-6$) are elastic constants. Minimization of $F_1[\eta(\xi), e_i] + F_1^{\text{el}}(e_i)$ with respect to the e_i yields the equilibrium values of the spontaneous secondary strains as functions of the effective order parameter η :

$$e_3^e = -\frac{\delta_1 \eta^2}{c_{11} - c_{12}}, \quad e_6^e = -\frac{\delta_2 \eta^2}{c_{44}}, \quad e_1^e = -\frac{\delta_3 \eta^2}{c_{11} + 2c_{12}}. \quad (31)$$

Introducing the preceding expressions of the e_i in $F_1(\eta, e_i)$ yields the renormalized order parameter expansion: $F_1[\eta(\xi)] = a_1 \eta^2 + \tilde{a}_2 \eta^4 + a_3 \eta^6$, where $\tilde{a}_2 = a_2 - \delta_1^2/(c_{11} - c_{12}) - \delta_2^2/c_{44} - \delta_3^2/(c_{11} + 2c_{12})$ is smaller than a_2 . Accordingly the renormalized height of the energy barrier is

$$h(e_i) = -\frac{2}{9} \eta_0^4 \left(\tilde{a}_2 + \frac{4}{3} a_3 \eta_0^2 \right) \quad (32)$$

which is lower than h . Hence, *the secondary strains favor the transformation from the bcc to the hcp phase*. This conclusion holds more generally for phase transformations of the reconstructive type and is consistent with the result obtained by Gooding *et al.*⁴⁰ in their model of the bcc-9R transformation.

At variance with a presupposed view that strongly first-order transitions imply strong anharmonicity of the lattice, let us now show that *martensitic reconstructive transformations may correspond to a jump between two harmonic potential wells*. In a phenomenological Landau-type approach an anharmonic behavior can be related to two main different situations.

(i) A single order parameter is associated with the transition. The anharmonicity is here expressed by the influence of the order parameter invariants of degrees higher than 2 in the thermodynamic potential and is reflected in the potential well by the existence of nonequidistant energy levels (frequencies) corresponding to transitions to different possibly stable states. A second-order transition is induced by a continuous variation of the potential profile through the flat bottom regime corresponding to a soft mode frequency $\omega_{\text{sm}} = 0$. The anharmonicity is weak in this case since it is essentially governed by the quadratic term in the potential. A first-order transition corresponds to a jump between two wells and the description of the changes in the potential profile requires anharmonic equations. However, this does not necessarily imply that the critical phonon displays anharmonicity as one has also to compare the soft mode frequency ω_{sm} and the height h of the energy barrier. If $\omega_{\text{sm}} \ll h$ the crystal will remain in the fully harmonic regime across the transition. If ω_{sm} is of the order of h an anharmonic regime should be observed for the critical phonon. Note that the phonon frequency should be more sensitive to temperature in this latter case.

(ii) More than one order parameter is required for the transition mechanism. The anharmonicity is then reflected also by the coupling invariants between the order parameters. The situation is more complex since the energy levels in the potential well possess nonzero widths and the soft modes can be associated with different wave vectors. However, similar conclusions can be drawn as in the single-order-parameter case taking into account the relative magnitude of the soft mode frequencies and of the height of the energy barrier.

Let us illustrate the preceding considerations by some numbers extracted from concrete examples of reconstructive bcc-hcp transformations. In Ba the value found for the jump in entropy⁴¹ which is expressed in our model by $\Delta S = -(\partial a_1 / \partial T) \eta^2(T_1)$ where T_1 is the bcc-hcp transition temperature gives $a_1 = -1.084 \text{ cal mol}^{-1} \text{ K}^{-1}$ and $a_2 = -0.084 \text{ cal mol}^{-1} \text{ K}^{-1}$. Assuming the normalizing values $\eta_0 = 1$ and $a_3 = 1$ one gets an estimate of the barrier height $h \approx 5 \text{ meV/atom}$. Since the order parameter keeps a constant value $\eta = \eta_0 = 1$ in the hcp phase the depth of the potential well [Fig. 14(c)] is $d = F_1(1) = a_1 + a_2 + a_3$. Its minimal value is reached on the second order transition line which separates in Fig. 14(a) the hcp and intermediate orthorhombic phases. The equation of this line is $a_1 = -2a_2 - 3a_3$ which gives $d_{\min} = -a_2 - 2a_3 \approx -25 \text{ meV/atom}$. Note that these estimates are in good agreement with the numbers found by Chen *et al.*⁴² from first principles total energy calculations ($h \approx 4 \text{ meV/atom}$, $d_{\min} \approx 27.2 \text{ meV/atom}$) confirming the consistency of our approach.

Comparing h and d_{\min} shows that the potential depth is about five times larger than the potential barrier. This ratio and the experimental value found for the frequency of the $T_1(N)$ phonon mode⁴² in Ba which is 3.1 meV suggest that the atoms are in a reasonably harmonic situation at the bcc-hcp transformation. In Zr,⁴¹ $\Delta S = -1.37 \text{ cal mol}^{-1} \text{ K}^{-1}$ from which one can deduce by analogous estimates $h \approx 14.5 \text{ meV/atom}$ and $d_{\min} \approx -69 \text{ meV/atom}$ which is of the same order as the value $d_{\min} \approx -45 \text{ meV/atom}$ obtained by pseudopotential calculations.⁴³ The depth of the well is again about five times larger than the barrier height. It reflects a strong harmonic regime when compared to the soft mode frequency⁴³ which is 4.17 meV . A similar conclusion can be drawn⁴⁴ for Ti in which the entropy jump⁴⁵ at the bcc-hcp transformation is: $\Delta S = -0.866 \text{ cal mol}^{-1} \text{ K}^{-1}$ corresponding to $h = 53.5 \text{ meV/atom}$ while the frequency of the soft mode⁴³ is $\sim 5 \text{ meV}$.

Coming back to the phase diagram of Fig. 14(a) we will now discuss in more detail the soft mode behavior when approaching the hcp phase from the bcc phase assuming that the transformation corresponds to a jump between two harmonic wells. In the following discussion the bcc, hcp, and intermediate orthorhombic phases are, respectively, denominated I, II, and III, and a_1 is assumed to symbolize the temperature axis.

For $a_2 > 0$ the second-order I-III transition takes place for $a_1 \sim \omega_{\text{sm}}^2 = 0$. The zero frequency line $a_1 = 0$ prolongates, for $-2a_3 < a_2 < 0$, onto the limit of stability between phase I and phase III. In this region the I-III phase transition becomes first order and the hardening of the soft mode reflects the increasing magnitude of the structural distortion of phase I in phase III. The maximum distortion is reached on the second-order transition line between phase III and phase II.

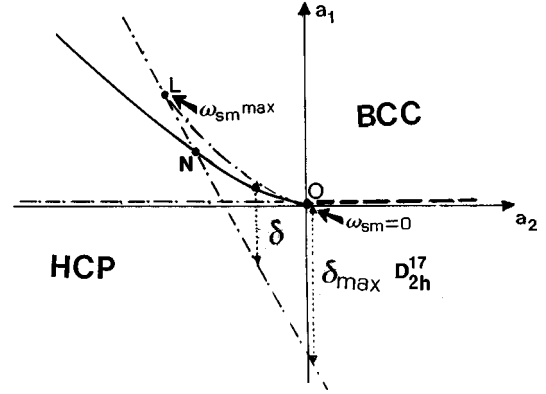


FIG. 15. Soft mode frequencies ω_{sm} along the transition lines separating the bcc phase from the hcp and intermediate phase. δ and δ_{\max} are used for an estimate of the partial softening [Eq. (33)].

Since phase II corresponds to a constant distortion (shifts) of phase I the soft mode frequency ω_{sm} reaches its maximum at the three-phase point N and then keeps a saturated value ω_{\max} across the reconstructive I-II transition. A rough estimate of the softening of the phonon mode when approaching phases II and III from phase I is the ratio $\delta / \delta_{\max} \approx (\Delta\omega/\omega)^2$ where δ and δ_{\max} represent the projections on the a_1 axis of the thermodynamic paths shown in Fig. 15, i.e., δ is the projection of the path between the limit of stability lines I-II and II-III, while δ_{\max} is the maximum value of δ reached for $a_2 = 0$. Using the equations of the limit of stability lines and the difference of their coordinates along the a_1 axis (Fig. 15) one finds

$$\frac{\delta}{\delta_{\max}} = \frac{3}{4} + \frac{3a_3(2a_2 + 3a_3)}{4(a_2 + 3a_3)^2}. \quad (33)$$

which varies from zero at the point L ($a_1 = a_3$, $a_2 = -2a_3$), where the stability lines I-II and II-III merge, to 1 at the origin ($a_1 = a_2 = 0$). In other words, no softening should take place beyond the L point ($\Delta\omega/\omega = 0$) whereas a maximum softening ($\Delta\omega/\omega = 1$) should occur at the origin. However, such behavior corresponds to an ideal limit situation (e.g., full harmonic regime, single order parameter with no coupling to secondary variables). For real reconstructive transitions it has to be interpreted in an extended and reciprocal way, namely, a *slight softening* of the phonon mode should be observed at a martensitic reconstructive transformation for thermodynamic paths close to the region of stability of the intermediate phase (III) whereas far from this region (for large negative values of a_2 in Fig. 15) *no softening should be observed*.

B. The phonon spectra of sodium and lithium

Let us describe the experimental results reported for the temperature dependence of the $\Sigma_4(qq0)$ phonon branch in sodium^{6,11,45,38,39} and lithium.^{7,9,13,15} In Na where the transformation occurs at about 34 K Blaschko and Krexner¹¹ find a softening of a portion of the phonon branch extending from 230 to about 40 K. The deepest softening ($\sim 4\%$) is disclosed around $q = 0.42$ but it exists from $q = 0.35$ ($\sim 2\%$) to the zone boundary N point ($\sim 3\%$). For smaller values of q no soften-

ing is detected and even a hardening below $q \sim 0.2$ is observed. The measurements of Abe *et al.*⁴⁵ essentially confirm the preceding results although the numbers found by these authors differ in the location of the deepest softening region which is found around $q \sim 0.33$ – 0.37 . Berliner *et al.*^{6,39} confirm a softening of a few percent from 200 to 30 K.

In lithium ($T_M = 74$ K) the experimental situation appears to be more contrasting. In their initial study Ernst *et al.*¹³ disclose a softening of almost the entire phonon branch, more pronounced around $q = 0.4$ ($\sim 13\%$) and the N point ($\sim 10\%$) and weaker around $q = 0.3$ ($\sim 3\%$) and $q = 0.2$ ($\sim 2\%$). In a further study Schwarz *et al.*¹⁵ observe different softening regimes depending on the distance to the martensitic transformation. After cooling from 200 to 100 K the softening extends from $q \geq 0.1$ to $q = 0.5$ ($\sim 6\%$) with an almost linear increase toward the zone boundary [Fig. 2(a) of Ref. 15]. Upon cooling from 200 to 80 K the softening extends to $q = 0.1$ and two distinct dips appear around $q = 0.3$ ($\sim 7\%$) and $q = 0.4$ ($\sim 8\%$) [Fig. 2(b) of Ref. 15]. When cooling from 100 to 80 K no softening is found below $q = 0.2$ and a single flat dip ($\sim 3\%$) remains, centered around $q = 0.33$ and extending from $q = 0.22$ to $q = 0.42$ [Fig. 2(c) of Ref. 15]. Smith⁷ finds at 100 K a softening of the Σ_4 branch between $q = 0.3$ and $q = 0.5$ (curve 3 in Ref. 7) which is more pronounced ($\sim 8\%$) at $q = 0.5$. No dip is seen by this author at $q = 0.4$. No evidence of even a slight dip at $q = 0.33$ is found by Smith *et al.*⁹

Let us note in a general way that the *existence* of a softening of the Σ_4 mode in the bcc phase above the martensitic transformations in Na and Li is a confirmation of the displacive character assumed for these transformations and of the possible contributions of secondary strains which are part of the full displacive mechanisms. As underlined in Sec. III A it also suggests that the region of stability of the martensite phases are not too far from the region of stability of the intermediate ‘‘Landau’’ phases assumed in the theoretical phase diagrams described in Sec. II. However, in the present case the *weakness* of the observed softening which is smaller than 4% in Na and smaller than about 10% in Li has obviously an additional source, i.e., the incomplete transformation of the bcc phase at low temperature. The *nonlocalized* (extended) character of the softening region on the Σ_4 branch reflects, on the one hand, the coexistence of different structures below the transformation which are associated with different q vectors and the strong coupling between the corresponding displacive mechanisms as assumed in our approach. It also denotes the possible existence of additional underlying transformation mechanisms (e.g., bcc-fcc) which do not necessarily give rise to the stabilization of a long-range order in the martensite phase.

In a more precise way the q interval of softening in Na extends approximately between the critical values associated with the $9R$ ($q = \frac{1}{3}$) and hcp ($q = \frac{1}{2}$) structures in agreement with the observation of these structures below the transition as reported by Schwarz *et al.*¹² By contrast, the stabilization of longer polytype structures ($27R, 15R, 45R$) proposed by Berliner *et al.*⁶ would require smaller q values (e.g., $q = \frac{1}{9}$ for a $27R$ polytype) corresponding to that part of the phonon branch which was experimentally observed to harden. The fact that longer polytypes are not reflected in the phonon spectrum can be explained by the fact that they require for

their formation a disordering mechanism which is triggered within the martensite without precursor indications in the bcc phase. This argument also holds for the disorder polytype structure evidenced in the lithium martensite which originates as described in Sec. II D from the disintegration of a fcc structure in contact with the $9R$ phase. Indication for the potential stabilization of a fcc structure below the bcc phase in Li is supported by the observation of Schwarz *et al.*¹⁵ of an extension of the q interval of softening below $q = 0.1$, i.e., close to the BZ center, when cooling from 200 to 80 K. The fact that the soft q interval becomes narrower and centered on $q = 0.33$ when cooling from 100 to 80 K shows that the tendency for the stabilization of the $9R$ structure becomes predominant in this region. An indirect confirmation that a dip at $q = \frac{1}{3}$ connects with the formation of a $9R$ martensite are the phonon measurements of Maier *et al.*⁴⁶ in Li-10 at. % Mg. In this system the close-packed low-temperature phase which appears about 90 K has a $9R$ structure over its entire range of stability at variance with the situation found in pure lithium. The relative phonon frequency shifts between 300 and 130 K clearly reveal a distinct dip of about 4% near $q = 0.3$. At last let us stress that the absence of even a slight dip around $q = \frac{1}{3}$ found by Smith *et al.*⁹ in Li may be explained by the abrupt first-order character reported by these authors for the bcc- $9R$ transformation while it is found to be moderately discontinuous in Refs. 11–15. This indicates that the transformation in Smith’s experiment possibly followed a thermodynamic path which is far from the region of coexistence with the intermediate Landau phase.

C. Precursor effects and the transformation mechanism

The most striking features of the soft-mode instabilities found in Na and Li are the extension of the softening region in q space and the fact that the q values corresponding to the observed dips are never located at the expected fractional values (e.g., $\frac{1}{3}$ for $9R$, $\frac{1}{2}$ for hcp) but are irrational numbers *close* to the preceding values. Furthermore, the locations of the dips show an evolution which seems to depend on the distance to the martensitic transformation and which is not exactly reproducible but depends on the history of the sample and on the thermodynamic paths. These facts which are reminiscent of the situation found in incommensurate structural transitions³ reflect a tendency to the formation of inhomogeneous structures. The strictly periodic (homogeneous) character of the structures appearing below the martensitic transformations in Na and Li can be attributed to the first-order nature of these transformations which realize an abrupt jump across the inhomogeneous region, squeezing an eventual structural modulation as it has been observed in a number of lock-in transitions^{3,4} between commensurate phases.

The question, however, arises to what extent the displacive (commensurate) mechanisms which have been depicted in Sec. II can be influenced by the potentially incommensurate character of the precursor instabilities, namely, if this character contributes to the complex nature of structures observed below the transformations and also explains the small discrepancies found in the different studies. Another crucial question concerns the possible origin of the incommensurability. Answers to these questions can be partly found in the

recent studies of Maier *et al.*^{46,48,49} which show the importance of coherency stresses related to the coexistence of the parent bcc structure with the “product” phases. A similar explanation was proposed for the stabilization of the 7R structure in NiAl described as an adaptive martensitic phase.⁵⁰

The bcc matrix which in most cases has transformed to about 50% never disappears at low temperatures. On the other hand, as shown in Sec. II, each of the low-temperature close-packed polytype structures, although they resemble each other and their energies are nearly degenerate,⁵¹ require for their formation secondary strains with different magnitudes. This leads to different coherency stresses with the bcc matrix which may result in the creation of strain fields with strain fluctuations acting inhomogeneously on the displacive transition order parameters. Phenomenologically, this is expressed by couplings between the space derivatives of the order parameter components and the strain components $e_{ij}(\partial\eta_k/\partial x_l)$ along the line of the model introduced for the description of the incommensurate structure which takes place between the α - and β -quartz structures.^{52,53} In the present case these couplings will only play a role for the dynamical behavior above the transformation and influence the transformation kinetics.

The importance of coherency stresses on the transformation kinetics is clearly demonstrated in the experiments of Maier *et al.*^{46,48,49} on lithium. In a first series of experiments⁴⁶ a [001] uniaxial stress was applied inducing a lattice expansion along [110] and changing the conditions defining coherency between the phases in the sense of a lowering of the coherency stresses. At 74 and 64 K the immediate response of the system to the applied stress is the formation of the low-temperature phase. In addition, at 64 K the amount of low-temperature phase formed increases roughly linearly with the applied deformation. Hence, a lowering of the coherency stresses promotes the phase transformation in a significant way. In another experiment⁴⁹ the response to the applied stress at 100 K is a softening of a few percent of the whole Σ_4 phonon branch, i.e., when the coherency stresses are released the whole set of close-packed structures become potentially stable.

When a stress is applied at 82 K, about eight degrees above the normal martensite temperature, to a virgin Li crystal the phase transformation takes place within a few minutes after about 5 h of incubation time.⁴⁶ The observation of incubation times, that was also reported⁴⁵ for Na at 38 K and in a deteriorated Li crystal⁹ at 65 K, as well as the precedingly mentioned data provide an insight into the specificity of the mechanism which connects the strain fluctuations to the nucleation process yielding the martensite formation. The strain fluctuations promoting the transition should be specific (e.g., of the [110] shear type) in order to favor the formation of a nucleus of the low symmetry phase. Once this nucleus is formed it induces a similar symmetry breaking deformation of the bcc matrix which likewise promotes the phase transformation in a self-amplification process of the transformation product due to its own strain field. This means that the transformation—once started—does not stop in an embryonic state but runs through the bcc matrix until it is arrested by the elastic energy of the two-phase boundary region.

When random strains (nonspecific) are present as in deteriorated crystals after one or several transformation cycles then, on the contrary, the nucleation is inhibited and consequently starts at lower temperatures. This is corroborated for example by the increase of the transformation hysteresis as experimentally observed by Maier *et al.*⁴⁹ in Li-10 at. % Mg.

The preceding scheme is also confirmed by the effects of plastic deformation on Li along [001] measured in Ref. 48. Below the phase transition temperature (74 K) plastic deformation favors the phase transformation but 30° above the transition temperature it inhibits the phase transformation even down to low temperatures. It can be conjectured that particles of the low-temperature phase persisting on heating do not act as centers of easy nucleation when the system is cooled down again, i.e., they are inactivated by the effect of the plastic deformation of the bcc matrix around the particles which reduces the specific elastic strain field needed for martensitic nucleation. As a consequence a significant density of embryos of the low-temperature phase should be present only close to the transformation in agreement with the observation of the diffuse scattering intensity delocalized in reciprocal space in the vicinity of the martensitic transformations in Li and Na.⁵⁴

It has to be stressed that the final structure of the martensite in Li and Na is not determined by the coherency stresses, but corresponds to an actual thermodynamic equilibrium state. This is illustrated for example by the results of Maier *et al.*⁴⁹ showing that in Li the deformation induced structure is similar to the structure obtained by a temperature change. Therefore, the general topology of the theoretical phase diagrams worked out in Sec. II is independent from the coherency stresses, which affect only the dynamical features of the transition. In contrast, the martensite structure is unstable with respect to plastic deformation. This is demonstrated by Maier *et al.*⁴⁹ who show that under severe plastic deformation the martensite is no longer 9R but a disordered polytype structure. Hence, the stacking order of the martensite that has been shown (Sec. III B) to partially disintegrate when the 9R and fcc structures coexist, becomes fully disintegrated under plastic deformation.

D. The nucleation process

The formation of martensitic embryos above the transformations in Li and Na does not necessarily require the existence of defects, i.e., the embryos may correspond to kinetically frozen-in Frenkel-type nuclei, due to thermal fluctuations.⁵⁵ In fact there are no direct observations showing the presence of defects in the two crystals above their transformations. Only indirect measurements in Li,⁵⁴ such as intensity streaks along the [110] direction and Huang scattering close to the transformation, suggest the presence of *small* defects. Although this interpretation needs further confirmation, let us show that the formation of embryos on elastic defects is consistent with the nucleation scheme described in the preceding section.

Assuming for simplicity a pure 9R structure for the martensite in Li and Na the nucleation process on elastic defects can be formalized using a Landau-Ginzburg free energy of the form⁵⁶

$$\begin{aligned} \tilde{\Phi}(\zeta, e_i) = \int_V \left[\Phi(\zeta, e_i) + F^{\text{el}}(e_i) + \lambda(\nabla\zeta)^2 \right. \\ \left. + F_{\text{in}} \left(\zeta, \frac{\partial\zeta}{\partial x_k}, e_i \right) \right] dV, \end{aligned} \quad (34)$$

where $\Phi(\zeta, e_i)$, given by Eq. (29), has the meaning of the free-energy *density* associated with the bcc-9R transformation. $F^{\text{el}}(e_i)$ is the elastic energy density expressed by Eq. (30). The λ term is the Ginzburg invariant which accounts for the order parameter fluctuations. F_{in} corresponds to the coupling between the space derivatives of the order parameter and the strain field reflecting the strain fluctuations which originate in the coherency stresses of the nuclei with the bcc matrix.

For the purpose of our demonstration we can restrict ourselves to consider a low degree coupling of the form

$$F_{\text{in}} \left(\zeta, \frac{\partial\zeta}{\partial x_k}, e_i \right) = f(\zeta) g \left(\frac{\partial\zeta}{\partial x_k} \right) (\mu_1 e_1 + \mu_2 e_6 + \mu_3 e_3), \quad (35)$$

where $g(\partial\zeta/\partial x_k)$ is a *linear* function of the space derivatives $\partial\zeta/\partial x_k$ and f is a function of the order parameter ζ . The Euler-Lagrange equation minimizing $\tilde{\Phi}$ can be written in this case

$$\begin{aligned} \lambda\Delta\zeta + \frac{1}{2} \sum_{i=1,3,6} \mu_i \nabla[f(\zeta)e_i] \\ = c_1\zeta + 2c_2\zeta^3 + 3c_3\zeta^5 + \frac{1}{2} g \nabla f \sum_{i=1,3,6} \mu_i e_i \\ + \zeta(\nu_1 e_1 + \nu_3 e_6) + \frac{3}{2} \zeta^2 e_3 \end{aligned} \quad (36)$$

and

$$\frac{\partial\sigma_{ik}}{\partial x_k} = 0, \quad (37)$$

where the σ_{ik} are the components of the internal stress tensor which are here

$$\begin{aligned} \sigma_{ii(i=1,2)} &= 3c_{12}e_{ii} + \nu_1\zeta^2 - \nu_2\zeta^3 + \mu_1fg, \\ \sigma_{33} &= (3c_{11} - 2c_{12})e_{33} + 2(\nu_1\zeta^2 + \nu_2\zeta^3) + fg(\mu_1 + 2\mu_3), \\ \sigma_{12} &= c_{44}e_{12} + \nu_3\zeta^2 + \mu_2fg, \\ \sigma_{13} &= \sigma_{23} = 0, \end{aligned}$$

where the e_{ij} are the components of the strain tensor. The system of Eqs. (36) and (37) has two types of solutions.

(1) $\zeta=0$ and $e_i = e_i^0(\mathbf{r})$, where $e_i^0(\mathbf{r})$ is the strain field associated with a defect above the onset of a nucleus, in the bcc phase.

(2) $\zeta = \zeta(\mathbf{r}) \neq 0$, $e_i = e_i^0(\mathbf{r}) + O(\zeta^2)$. This corresponds to a state with a nucleus on the defect in the bcc phase, below the nucleation temperature T_n .

The preceding solutions coincide with different positive values of the coefficient $c_1 = c(T - T_m)$, where T_m is the martensitic transformation temperature. In order to determine

the critical value C_1^n at which the nucleus arises in the bcc phase, which corresponds to the bifurcation between the solutions (1) and (2), one has to linearize Eqs. (36) and (37) around $\zeta=0$ and $e_i^0(\mathbf{r})$ following the method developed in Ref. 57. Assuming that $f(\zeta)$ can be approximated to the lowest order by a linear term $f(\zeta) \sim A\zeta$, the linearization results in the equation

$$\begin{aligned} \lambda\Delta\psi_n + \frac{A}{2} \sum_{i=1,3,6} \mu_i \nabla[e_i^0(\mathbf{r})\psi_n] \\ = [C_1^n + \nu_1 e_1^0(\mathbf{r}) + \nu_3 e_6^0(\mathbf{r})]\psi_n, \end{aligned} \quad (38)$$

where ψ_n is the eigenfunction corresponding to the first eigenvalue $C_1^n = C(T_n - T_m)$, T_n being the nucleation temperature. Following Ref. 57, the main term of the branched off solution of Eq. (38) can be written

$$\eta = \xi\psi_n(\mathbf{r}) + O(\xi^3). \quad (39)$$

and

$$e_i(\mathbf{r}) = e_i^0(\mathbf{r}) + \frac{K_i \xi^2}{(2\pi)^3} \int G_{ik}(\mathbf{k}) k_i k_k Q(\mathbf{k}) \exp(i\mathbf{k}\mathbf{r}) d^3k, \quad (40)$$

where ξ represents a normalizing amplitude. The Fourier transform in Eq. (40) expresses the contribution of the strain e_i induced by the nucleus. $G_{ik}(\mathbf{k})$ is the elastic Green function and $Q(\mathbf{k}) = \int \psi_n^2 \exp(-i\mathbf{k}\mathbf{r}) d^3r$. The asymptotic solution of Eqs. (39) and (40) is

$$\eta \sim \xi \exp\left(\frac{-r}{r_n}\right). \quad (41)$$

The radius r_n of the nucleus is given by

$$r_n = \frac{\lambda}{c} (T_n - T_m)^{-1/2} + K, \quad (42)$$

where K is a constant. Equation (42) shows that for a nucleus arising far from the martensitic transformation, i.e., for large values of $T_n - T_m$, the λ term is small, and the radius r_n is almost constant. In contrast, when the nucleus appears close to the martensitic transformation, i.e., for small values of $T_n - T_m$, the λ term in Eq. (42) predominates, the size of the nucleus increasing upon approaching T_m . This picture is consistent with the qualitative interpretation given in Sec. III C for the experiments of Maier *et al.*⁴⁷⁻⁴⁹ Far from T_m the nuclei are inhibited and do not trigger the transformation mechanism, whereas close to T_m the nucleation process promotes the transformation. Note that the considerations leading to Eq. (42) are independent of the nature of the defects on which depend the particular form of ψ_n and the value of C_1^n .

IV. SUMMARY AND CONCLUSION

In the theoretical description proposed in this article for the martensitic transformations in sodium and lithium, two types of results can be distinguished.

(1) Results which are deduced from the reconstructive character of the transformations and apply more generally to

any transformation between structures which are not group-subgroup related.³ These results can be summarized as follows.

(a) The mechanisms associated with the bcc-9R, bcc-hcp, and bcc-fcc transformations involve specific critical atomic displacements, the corresponding order parameter moduli being periodic functions of the critical displacements.

(b) The transformation mechanisms require additional spontaneous strains (e_3, e_6, e_1) which, for specific magnitudes, are also symmetry-breaking quantities although they can be treated, in the framework of a Landau-type approach, as secondary order parameters.

According to these results, the 9R, hcp, and fcc phases appear as *limit* phases which are realized for definite values of the critical shifts and strains. This essential feature entails other properties of reconstructive transformations.

(c) The theoretical phase diagrams associated with the transformations involve intermediate phases having the maximal substructure common to the initial (bcc) and final (9R, hcp, or fcc) structures. These phases are obtained for general (nonspecific) displacements in the direction of the critical shifts and do not require, for their stability, additional secondary strains.

(d) The existence of a softening of the Σ_4 phonon branch as a precursor to the transformation depends on the vicinity to the preceding intermediate phase, on the thermodynamic path followed in the experiment. If the path is close to its region of stability, a partial softening should be observed, whereas far from this region no softening should occur. On the other hand, reconstructive transitions are not necessarily associated with a strong anharmonicity of the lattice and may correspond to a jump between harmonic potential wells. This jump is favored by the secondary strains.

(2) A second series of results are proper to the situation found in Na and Li.

(a) The complex structures found for the martensite phases result from a coupling between two, and possibly three different mechanisms. For Na the coupling concerns the bcc-9R and bcc-hcp transformation mechanisms, whereas the bcc-fcc mechanism may also be involved for Li. Besides, the existence of a fcc structure on heating in Li has been shown to originate in the disordered polytype structure found below the transformation and, resulting from a disintegration of the fcc and hcp structures, due to the contact with the 9R structure. The interplay between displacive and ordering processes is in the nature of reconstructive transformations to close-packed structures.

(b) There is no contradiction in the results reporting the absence of precursor mode softening, or a weak softening, since the corresponding experimental paths may be situated at different distances from the region of stability of the intermediate phase. The nonlocalized character of the softening region on the Σ_4 branch reflects the coupling between various structural mechanisms. The fact that the q values correspond to irrational numbers, whose values depend on the history of the sample and the experimental paths, is interpreted by a potential incommensurate character of the transformation. This character is attributed to different coherency stresses between the potentially stable structures and the bcc matrix, which results in the creation of strain fields acting inhomogeneously on the effective order parameter. This influences the other features of the transformations, namely, the incubation times and the response of the crystals to elastic and plastic deformations. A nucleation process on elastic defects, which is activated only close to the martensitic transformation, has been shown to be consistent with the preceding properties.

The phenomenological model developed in the present work provides a coherent framework for reconciling the apparently contradictory observations reported by Smith, Blaschko, and their co-workers. However, it is beyond the scope of a phenomenological approach to explain *why*, in contrast to other reconstructive transformations in metals,³ the martensitic transformations in Na and Li display such unusual and complex features. Possibly, the answer to this question may be found in the fact that Na and Li possess unique mechanical properties. In this respect, it was recently pointed out by Pichl and Krystian⁵⁸ that the flow-stress versus temperature curves of Li and Na differ from those of all other bcc metals: The temperature range in which the flow stress is usually controlled by thermally activated kink pair formation in screw dislocations cannot be reached in the bcc phase, and in spite of that, a large plastic anisotropy is observed in this phase. In simpler words, the complexity of the transformation features of Li and Na would be related to the particular *softness* of their crystalline state which, in particular, may result in the fact that the bcc phases never completely transform into the martensite phase.

ACKNOWLEDGMENTS

The theoretical model developed in this article has been motivated by the many discussions with Oskar Blaschko. Our work was partly supported by the Fonds zur Förderung der wissenschaftlichen Forschung in Austria.

*On leave from the University of Amiens, France.

¹Z. Nishiyama, *Martensitic Transformations* (Academic, New York, 1978).

²L. R. Testardi, *Phys. Acoust.* **10**, 193 (1973).

³P. Tolédano and V. Dmitriev, *Reconstructive Phase Transitions* (World Scientific, Singapore, 1996), Chap. 3.

⁴J. C. Tolédano and P. Tolédano, *The Landau Theory of Phase Transitions* (World Scientific, Singapore, 1987), Chap. 3.

⁵H. G. Smith, R. Berliner, J. D. Jorgensen, and J. Trivisonno, *Phys. Rev. B* **43**, 4524 (1991).

⁶R. Berliner, H. G. Smith, J. R. D. Copley, and J. Trivisonno,

Phys. Rev. B **46**, 14 436 (1992).

⁷H. G. Smith, *Phys. Rev. Lett.* **58**, 1228 (1987).

⁸H. G. Smith, R. Berliner, J. D. Jorgensen, M. Nielsen, and J. Trivisonno, *Phys. Rev. B* **41**, 1231 (1990).

⁹H. G. Smith, R. Berliner, and J. Trivisonno, *Phys. Rev. B* **49**, 8547 (1994).

¹⁰R. Berliner, O. Fajen, H. G. Smith, and R. L. Hitterman, *Phys. Rev. B* **40**, 12 086 (1989).

¹¹O. Blaschko and G. Krexner, *Phys. Rev. B* **30**, 1667 (1984).

¹²W. Schwarz, O. Blaschko, and I. Gorgas, *Phys. Rev. B* **46**, 14 448 (1992).

- ¹³G. Ernst, C. Artner, O. Blaschko, and G. Krexner, *Phys. Rev. B* **33**, 6465 (1986).
- ¹⁴W. Schwarz and O. Blaschko, *Phys. Rev. Lett.* **65**, 3144 (1990).
- ¹⁵W. Schwarz, O. Blaschko, and I. Gorgas, *Phys. Rev. B* **44**, 6785 (1991).
- ¹⁶C. S. Barrett and O. R. Trautz, *Trans. Am. Inst. Min. Metall. Pet. Eng.* **175**, 579 (1948).
- ¹⁷C. S. Barrett, *Acta Crystallogr.* **9**, 671 (1956).
- ¹⁸C. M. McCarthy, S. W. Tomson, and S. A. Werner, *Phys. Rev. B* **22**, 574 (1980).
- ¹⁹A. W. Overhauser, *Phys. Rev. Lett.* **53**, 64 (1984).
- ²⁰O. V. Kovalev, *Irreducible Representations of the Space Groups* (Gordon and Breach, New York, 1969).
- ²¹W. G. Burgers, *Physica (Amsterdam)* **1**, 56 (1934).
- ²²V. P. Dmitriev, Yu. M. Gufan, and P. Tolédano, *Phys. Rev. B* **44**, 7248 (1991).
- ²³V. P. Dmitriev, S. B. Rochal, Yu. M. Gufan, and P. Tolédano, *Phys. Rev. Lett.* **60**, 1958 (1988).
- ²⁴E. G. Bain, *Trans. AIME* **70**, 25 (1924).
- ²⁵H. Warlimont and L. Delaey, *Martensitic Transformations in Copper, Silver and Gold Based Alloys* (Pergamon, Oxford, 1974), Chap. 3.
- ²⁶W. H. Zachariasen, *Acta Crystallogr.* **5**, 19 (1952).
- ²⁷U. Benedict, in *Handbook on the Physics and Chemistry of the Actinides*, edited by A. J. Freeman and G. H. Lander (Elsevier, Amsterdam, 1987).
- ²⁸B. Mettout, V. P. Dmitriev, M. Ben Jaber, and P. Tolédano, *Phys. Rev. B* **48**, 6908 (1993).
- ²⁹D. A. Young, *Phase Diagrams of the Elements* (University of California Press, Berkeley, 1991).
- ³⁰J. A. Wilson and M. de Podesta, *J. Phys. F* **16**, L121 (1986).
- ³¹L. D. Landau and E. M. Lifshitz, *Quantum Mechanics* (Pergamon, New York, 1965).
- ³²R. G. Gooding and J. A. Krumhansl, *Phys. Rev. B* **38**, 1695 (1988).
- ³³A. R. Verma and P. Krishna, *Polymorphism and Polytypism in Crystals* (Wiley, New York, 1966).
- ³⁴N. V. Belov, *Structure of Inorganic Crystals and Metallic Phases* (ANSSSR, Moscow, 1947).
- ³⁵V. P. Dmitriev, S. B. Rochal, Y. M. Gufan, and P. Tolédano, *Phys. Rev. Lett.* **62**, 2495 (1989).
- ³⁶H. Jagodzinski, *Acta Crystallogr.* **7**, 300 (1954).
- ³⁷R. Berliner and S. A. Werner, *Phys. Rev. B* **34**, 3586 (1986).
- ³⁸O. Blaschko and G. Krexner, *Phys. Rev. B* **51**, 16 464 (1995).
- ³⁹R. Berliner, H. G. Smith, J. R. D. Copley, and J. Trivisonno, *Phys. Rev. B* **51**, 16 467 (1995).
- ⁴⁰R. G. Gooding, Y. Y. Ye, C. T. Chou, K. M. Ho, and N. B. Harmon, *Phys. Rev. B* **43**, 13 626 (1991).
- ⁴¹E. Yu. Tonkov, *High Pressure Phase Transformations* (Gordon and Breach, Philadelphia, 1992).
- ⁴²Y. Chen, K. M. Ho, and B. N. Harmon, *Phys. Rev. B* **37**, 283 (1988).
- ⁴³K. M. Ho, C. L. Fu, and B. N. Harmon, *Phys. Rev. B* **29**, 1575 (1984).
- ⁴⁴W. Petry, A. Heiming, J. Trampenau, M. Alba, C. Herzig, H. R. Schober, and G. Vogl, *Phys. Rev. B* **43**, 10 948 (1991); J. Trampenau, A. Heiming, W. Petry, M. Alba, C. Herzig, W. Miekeley, and H. R. Schober, *ibid.* **43**, 10 963 (1991).
- ⁴⁵H. Abe, K. Oshima, T. Suzuki, S. Hoshino, and K. Kakurai, *Phys. Rev. B* **49**, 3739 (1994).
- ⁴⁶Ch. Maier, R. Glas, O. Blaschko, and W. Pichl, *Phys. Rev. B* **51**, 779 (1995).
- ⁴⁷Ch. Maier, O. Blaschko, and W. Pichl, *Phys. Rev. B* **52**, 9283 (1995).
- ⁴⁸Ch. Maier, O. Blaschko, and W. Pichl, *Phys. Rev. B* **55**, 113 (1997).
- ⁴⁹Ch. Maier, O. Blaschko, and W. Pichl, *Phys. Rev. B* **55**, 12 062 (1997).
- ⁵⁰A. G. Khachatryan, S. M. Shapiro, and S. Semenovskaya, *Phys. Rev. B* **43**, 10 832 (1991).
- ⁵¹A. Zangwill and R. Bruinsma, *Comments Condens. Matter Phys.* **13**, 1 (1987).
- ⁵²T. A. Aslanyan and A. P. Levanyuk, *JETP Lett.* **28**, 70 (1978).
- ⁵³T. A. Aslanyan, A. P. Levanyuk, M. Vallade, and J. Lajzerowicz, *J. Phys. C* **16**, 6707 (1983).
- ⁵⁴O. Blaschko, *Mater. Sci. Eng., A* **127**, 257 (1990).
- ⁵⁵A. L. Roitburd, *Phys. Status Solidi A* **40**, 333 (1977).
- ⁵⁶A. A. Boulbitch and P. Tolédano, *Phys. Rev. Lett.* **81**, 838 (1998).
- ⁵⁷M. M. Vajnberg and V. A. Trenogin, *Theory of Branching of Solutions of Non-Linear Equations* (Noordhoff, Leyden, 1974).
- ⁵⁸W. Pichl and M. Krystian, *Phys. Status Solidi A* **160**, 373 (1997).